

APPENDIX

Ferroelectrics, 414:140–146, 2011
Copyright © Taylor & Francis Group, LLC
ISSN: 0015-0193 print / 1563-5112 online
DOI: 10.1080/00150193.2011.577328



The Role of Vacancy Defects on the Dynamic Hysteresis Properties of Ferroelectric Thin Films: Monte Carlo Simulation with the DIFFOUR Model

SITTIDET SRINOI^{1,2,*} AND YONGYUT LAOSIRITAWORN^{1,2}

¹Department of Physics and Materials Science, Faculty of Science, Chiang Mai University, Chiang Mai 50200, Thailand

²Thailand Center of Excellence in Physics (ThEP), Commission on Higher Education, Bangkok 10400, Thailand

In this work, the effect of random vacancy defects on the electrical properties of ferroelectric thin-films was studied. The Monte Carlo simulation, based on the ferroelectric DIFFOUR model, was performed in the lattice system with free and periodic boundary conditions. The Metropolis algorithm was considered in choosing the proper states under the presence of the electric field. From the results, the hysteresis area at a given field was found to depend on the thickness of thin films and the vacancy defects of system. For instance, in thicker films, the larger hysteresis area was observed, which is resulted from the stronger ferroelectric interaction. On the other hand, the hysteresis area decreases with increasing vacancy concentration, due to the reduction of ferroelectric interaction on the average. To understand the hysteresis behaviors, the scaling exponents of associated parameters in the power law scaling form were considered. The results were discussed and compared with these from literatures.

1. Introduction

The dynamic hysteresis has now been considered important in both fundamental and technological point of view in terms of their associates, such as hysteresis shape, loop area, remnant polarization, coercivity field. For instance, the hysteresis area is the energy dissipated within one cycle of dipole switching, which identifies the nature of phase transition between ferro- and para-phase. Moreover, the remanence and coercivity show the stability of the ordered alignment at nonzero temperature. The studies in such a topic become interesting subject from the point of view of applications, due to the high-speed memory devices in which ferroelectric thin films are being developed extensively [1]. Therefore, the responses of ferroelectric thin films to external field including films structure, such as thin film's thickness, were investigated in detail to design better devices [2, 3]. However, the roles of hysteresis on electrical properties of ferroelectric thin films affected by the external applied field have not been quite well recognized, due to the complexity of thin films structure, and dynamic hysteresis has received less emphasis [4–6]. Although a number of the defect-free systems had been investigated and reported [7–11], a more realistic model which includes the effects of the defects, especially the non-electric inclusion, has

Received June 20, 2010; in final form July 9, 2010.

*Corresponding author. E-mail: sittidet99@hotmail.com

not been studied, in details. In this work, the Monte Carlo simulation [12] was employed to investigate the electrical properties of ferroelectric thin films with internal vacancy defects. The purpose is to obtain a more detailed understanding of how both defect concentration and film thickness affect the hysteresis properties.

2. Methodology

In this work, the DIFFOUR model with an inclusion of non-electric-sites was considered. The Hamiltonian was written as [13, 14]

$$H = \sum_i \left(\frac{P_0^2}{2m} - \frac{a}{2} u_i^2 + \frac{b}{2} u_i^4 \right) - U \sum_{\langle ij \rangle} \vec{u}_i \cdot \vec{u}_j - \vec{E}(t) \cdot \sum_i \vec{u}_i, \quad (1)$$

where $P_0^2/2m$ denotes the kinetic energy, \vec{u}_i is the ferroelectric dipole at site i and is considered to be a vector with constant magnitude, a and b are the double-well potential parameters, $\langle ij \rangle$ means the summation taking over the nearest neighbors pairs of dipoles, U refers to the ferroelectric interaction and $\vec{E}(t) = E_0 \sin(2\pi ft)\hat{z}$ represents an external electric field acting only on the z -direction of thin-films, where E_0 and f are field amplitude and frequency respectively. The Hamiltonian in Eq. (1) can be simplified by using the appropriate reference energy, and as $|\vec{u}_i|$ is constant in magnitude (to emphasize effects of domain reorientation), Eq. (1) can be rewritten as

$$H = -U \sum_{\langle ij \rangle} \hat{u}_i \cdot \hat{u}_j - E(t) \sum_i u_{iz}, \quad (2)$$

where \hat{u}_i is a unit vector having to one of the possible 14 ferroelectric dipole directions (8 from rhombohedral and 6 from tetragonal structures). The magnitude of each dipole was absorbed into U , and u_{iz} is the z -component dipole at site i . Moreover, U was used as the unit of energy, therefore the unit of temperature T and electric field E were redefined as U/k_B and U respectively, where k_B is the Boltzmann's constant.

In preparing the system, the ferroelectric dipoles were assumed to reside in the unit cells the considered ferroelectric lattice system consisting of $N = L \times L \times l$ dipoles, where $L \times L$ denotes a film's size and l is the ideal-film thickness (the number of monolayer) and N refers to the total ferroelectric dipoles. Here, l is chosen to be 1, 2, 4, 6 and 8. $L \gg l$ was chosen to preserve the film geometry. Therefore, $L = 100$ was considered where results from larger sizes were not significantly different. The Metropolis algorithm [15] was considered and periodic and free boundary conditions were used along the xy -plane (in-plane direction) and the z -direction (out-of-plane direction). Moreover, the defect concentrations (non-electric sites) of system c , included into the structure varies from $c = 0, 1, 4, 6, 10$ and 20%.

In updating the dipole configuration, a dipole \hat{u}_i was randomly chosen and assigned a new random direction (from possible 14 directions). The new direction was accepted with the following Metropolis algorithm

$$prob = \begin{cases} \exp(-\Delta H_i(t)/k_B T) & \text{if } \Delta H_i(t) > 0 \\ 1 & \text{if } \Delta H_i(t) \leq 0 \end{cases}, \quad (3)$$

where $\Delta H_i(t)$ is the energy difference due to the update at site i and time t . The unit time was scaled in unit of Monte Carlo step per sites (mcs), which is equivalent to N trial updates.

The site \hat{u}_i was updated if $\Delta H_i(t) \leq 0$ or random number $r < prob$, where $r \in [0, 1)$. These procedures were repeated until the simulation terminates.

In measuring the observables, a fixed temperature $T = 0.5 U/k_B$ was chosen since all considered ferroelectric films are in their ferroelectric phase at this T [16]. Moreover, a given fixed field $E_0 = 4.0 U$ was considered to investigate how the other parameters affect the hysteresis behaviors. Therefore, with varying l, f , and c , the hysteresis loops were drawn by calculating the polarization per dipole at time t , i.e.

$$p(t) = \frac{1}{N'} \sum_i u_{iz}(t), \quad (4)$$

where N' is the total number of available dipoles. The first 1000 hysteresis loops were discarded for the steady state condition, and next 10000 loops were performed to average the hysteresis area

$$A = \oint p dE \quad (5)$$

In this work, f varied from 0.010 to 1.000 mcs^{-1} .

3. Results and Discussions

Figure 1(a) presents the simulated hysteresis loops, which was performed on 2 layered films, at a series of frequencies f but fixed $E_0 = 4.0 U$. The system without the vacancy defects was considered. From the results, at low frequency (or large period), the hysteresis shape looks like a thin rhombic pattern or s -shape loop, but as frequency increases, hysteresis loops reduce along polarization axis since the phase-lag is large. This is as with faster field switching, the dipoles have less time to respond the field change.

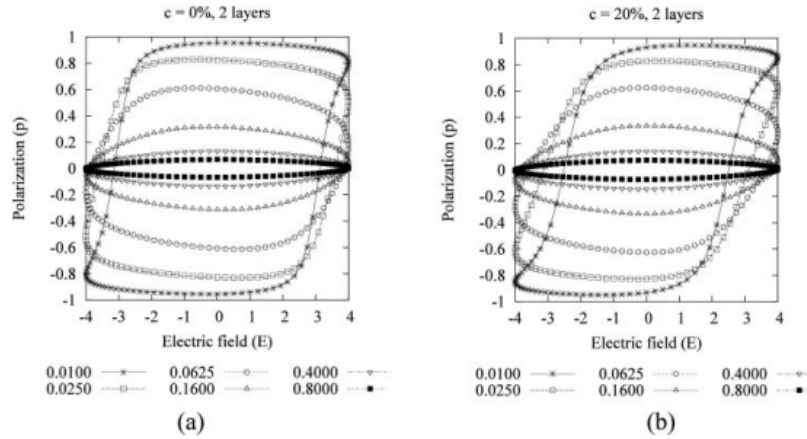


Figure 1. The hysteresis loops of (a) perfect structure and (b) defected system $c = 20\%$ with varying frequency f from 0.010 to 0.800 mcs^{-1} at $l = 2$, $T = 0.5 U/k_B$.

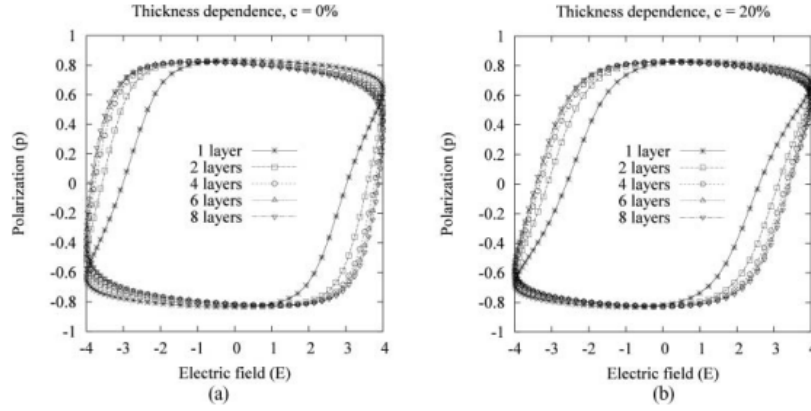


Figure 2. The thickness dependence of hysteresis loops at (a) $c = 0$ and (b) $c = 20\%$ and l varies from 1 to 8 layers at $f = 0.025 \text{ mcs}^{-1}$.

The effect of vacancy defect with $c = 20\%$ on hysteresis loops were shown as Fig. 1(b). From the results, the hysteresis loop, e.g. at $f = 0.010 \text{ mcs}^{-1}$ was slimmer compared to the ideal structure case, and so does hysteresis area since the ferroelectric interaction was decreased on the average due to some dipoles missing. The energy dissipated in dipole switching was also decreased.

From the results of perfect structure, the layer dependence of hysteresis loops at fixed frequency $f = 0.025 \text{ mcs}^{-1}$ and field amplitude $E_0 = 4.0 U$ was exhibited in Fig. 2(a). It was found that, at $l = 1$, the hysteresis shape look likes a slim s -shape. However, for $l \geq 2$, the hysteresis loops are similar to oval-shape loop due to the stronger ferroelectric interaction, in enhancing the phase-lag, and the energy dissipated in changing the dipole's direction is larger. Figure 2(b) shows the hysteresis loops of structure with vacancy defect $c = 20\%$. The results are similar to the perfect structure, but the hysteresis areas are smaller due to the weaker ferroelectric interaction.

To investigate how hysteresis area responds to the field frequency f , the film's thickness l and the defect concentration c , the hysteresis area A as function of f , l and c were calculated. Examples were shown in Fig. 3(a) and Fig. 3(b). Both of them displayed the qualitatively same area profile, that is, A gets increasing at thicker films due to stronger ferroelectric interaction and decreasing at low frequency region ($f < 0.1 \text{ mcs}^{-1}$), with higher concentration c , i.e. Fig. 2(b), less area was observed due to the weaker ferroelectric interaction. Then at high frequency region ($f > 0.1 \text{ mcs}^{-1}$), A decreases in this very high frequency region and become less dependent of l and c because the system have less time to switch the dipoles of system. These results are consistent with the hysteresis results in Figs. 1 and 2.

It is also of interest to introduce the empirical scaling relation in power law, i.e.

$$A \propto f^\alpha l^\beta (1 - c)^\gamma, \quad (6)$$

where α , β and γ are the exponents to scaling. These exponents imply how the hysteresis area (or the dissipation energy) responds to f , l and c . The appropriate fit was obtained at high f ($> 0.100 \text{ mcs}^{-1}$) as there is not enough data for the fit in the low f region. Results and

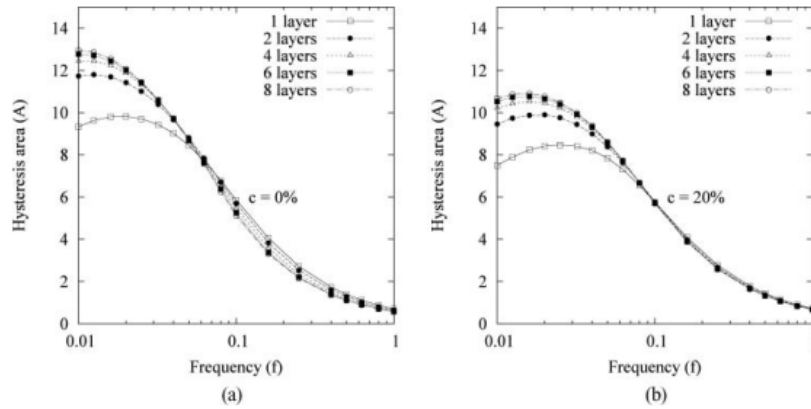


Figure 3. The frequency dependence of hysteresis area at (a) $c = 0\%$ and (b) $c = 20\%$, l ranges from 1 to 8 layers.

their good R^2 were shown in Fig. 4, where good their R^2 confirm the scaling accuracy with the exponents $\alpha = -0.979$, $\beta = -0.082$ and $\gamma = -0.114$. According to the previous work [16], without any defects in considered system, the scaled exponents of f and l were -0.969 and -0.028 respectively. These results show that the area A decreases with increasing f and l .

The remnant polarization p_r and coercive field E_c were also discussed in this work via slim hysteresis loops shown in Fig. 5. When the external electric field drops to zero, the

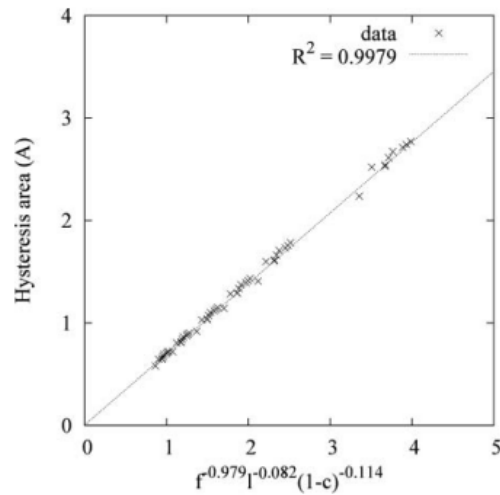


Figure 4. The scaling between A and $f^{-0.979}l^{-0.082}(1-c)^{-0.114}$ for $f > 0.100 \text{ mcs}^{-1}$.

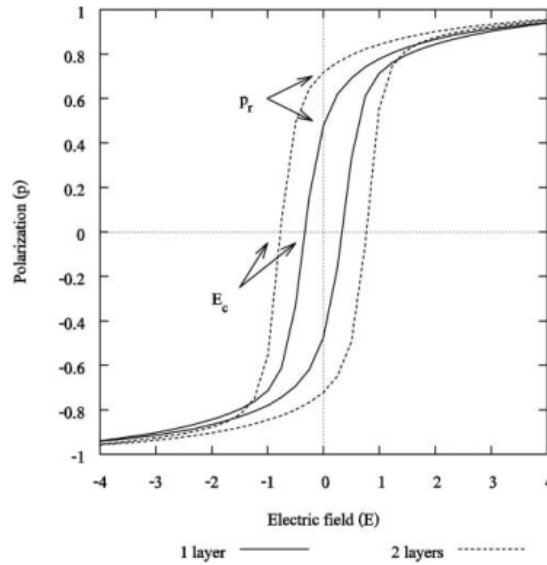


Figure 5. The slim hysteresis loop simulated at $f = 0.0010 \text{ mcs}^{-1}$, $E_0 = 4.0 U$, $T = 1.0 U/k_B$ and $c = 0\%$ for 1 and 2 layers respectively.

system retains a nonzero polarization or p_r since it does not relax back to zero polarization since dipoles require more time to respond the field change. (This is useful as a memory device). To switch the polarization back to zero, the coercive field E_c is required. Both p_r and E_c can be positive and negative values. In addition, p_r increases in thicker films and so does E_c due to the larger number of dipoles and stronger ferroelectric interaction. Therefore, the imposed electric field have to be increased to switch the polarization to zero.

4. Conclusions

The hysteresis behaviors of ferroelectric thin films with vacancy defects were investigated by Monte Carlo simulation. The DIFFOUR model was employed in this work and Metropolis algorithm was considered to update the system. The evolution of hysteresis loops was simulated to investigate the hysteresis behavior. The layer and frequency dependence of hysteresis loop and the frequency dependence of hysteresis area were found, and the power law relation among the hysteresis area, the field frequency, and the vacancy concentration, was proposed. The remnant polarization and coercive field were also discussed.

Acknowledgment

The authors would like to acknowledgment financial supports from the Graduate School of Chiang Mai University, Industry/University Cooperative Research Center (I/UCRC) in HDD Component, the Faculty of Engineering, Khon Kaen University and National Electronics and Computer Technology Center, National Science and Technology Development Agency.

References

1. J. F. Scott, *Ferroelectric Memories* (Springer-Verlag, Berlin, 2002).
2. A. Murayama, K. Hyomi, J. Eickmann, and C. M. Falco, *Phys. Rev. B* **61**, 8984 (2000).
3. M. T. Johnson, P. J. H. Bloemen, F. J. A. d. Broeder, and J. J. d. Vries, *Rep. Prog. Phys.* **59**, 1409 (1996).
4. M. Rao, H. R. Krishnamurthy, and R. Pandit, *Phys. Rev. B* **42**, 856 (1990).
5. J.-S. Suen and J. L. Erskine, *Phys. Rev. Lett.* **78**, 3567 (1997).
6. F. Zhong, J. Dong, and D. Y. Xing, *Phys. Rev. Lett.* **80**, 1118 (1998).
7. M. Abel and R. Siems, *Ferroelectrics* **126**, 275 (1992).
8. W. Cao and L. E. Cross, *Phys. Rev. B* **44**, 5 (1991).
9. J.-M. Liu and Z. G. Liu, *Mater. Lett.* **36**, 17 (1998).
10. S. Nambu and D. A. Segala, *Phys. Rev. B* **50**, 5838 (1994).
11. B. G. Potter, Jr., V. Tikare, and B. A. Tuttle, *J. Appl. Phys.* **87**, 4415 (2000).
12. M. E. J. Newman and G. T. Barkema, *Monte Carlo Methods in Statistical Physics* (Oxford University Press Inc., New York, 1999).
13. T. Janssen and J. A. Tjon, *Phys. Rev. B* **24**, 2245 (1981).
14. J.-M. Liu, Q. C. Li, W. M. Wang, X. Y. Chen, G. H. Cao, X. H. Liu, and Z. G. Liu, *J. Phys.: Condens. Matt.* **13**, L153 (2001).
15. N. Metropolis, A. W. Rosenbluth, M. N. Rosenbluth, A. H. Teller, and E. Teller, *J. Chem. Phys.* **21**, 1087 (1953).
16. Y. Laosiritaworn, *Key Eng. Mater.* **421–422**, 177 (2009).

Ferroc Hysteresis Modeling

S. SRINOI,^{1,2} K. KANCHIANG,^{1,2} W. LAOSIRITAWORN,³
R. YIMNIRUN,⁴ AND Y. LAOSIRITAWORN^{1,2,*}

¹Department of Physics and Materials Science, Faculty of Science, Chiang Mai University, Chiang Mai 50200, Thailand

²Thailand Center of Excellence in Physics, Commission on Higher Education, Ministry of Education, Bangkok 10400, Thailand

³Department of Industrial Engineering, Faculty of Science, Chiang Mai University, Chiang Mai 50200, Thailand

⁴School of Physics, Institute of Science, Suranaree University of Technology, Nakhon Ratchasima 30000, Thailand

Ferroc hysteresis modeling is an approach applicable to study lagging relationship between ferroc properties and external-dynamic-perturbation behaviors. The understanding to the lagging hysteresis behaviors, such as hysteresis area, coercive field, or remnant magnetization/polarization, is essential to the material-industry development. In this review, fundamental analysis as a microscopic study, including spin models, mean-field method and Monte Carlo simulation, and data processing analysis as a linking bridge between macroscopic analysis and the experiment results, such as the artificial neural network (ANN) and Fourier analysis, were elaborated on how they can be used to model the dynamic ferroc hysteresis. Then, ferroc behaviors were explained on how they depend on the external perturbations, such as the field parameters and temperature. The responses of ferroc behaviors on these factors, in both qualitatively and quantitatively, were also discussed in details.

Keywords Ferroc hysteresis; spin model; mean-field analysis; Monte Carlo simulation; artificial neural network; Fourier transformation

1. Introduction

Ferroc is a generic name given to groups of ferroelectric, ferromagnetic, and ferroelastic materials, and associated ferro-type behavior. The comprehensive understanding in ferroc behaviors is very essential for making the best use of complex materials in applications. For instance, the ferroc materials have been used as vital compositions in some smart-structure applications, such as sensors and actuators [1]. In addition, during recent years, ferroc materials also play an important role in developing the memory media for modern technology era, such as ferroelectric materials in high-speed nonvolatile memory application [2], ferromagnetic materials in high-density magnetic recording media [3], and ferroelastic materials in shape memory alloys (SMAs)—a material that can retain to its original geometry after deformation [4, 5].

Received in final form March 27, 2011.

*Corresponding author. E-mail: yongyut.laosiritaworn@yahoo.com

In general, ferroic materials are sensitive to external perturbations e.g. temperature T , electric field E , magnetic field h , or stress σ . When ferroic materials are subjected to a time-dependent oscillatory external field, they exhibit a history-dependent behavior called hysteresis. Typically, behaviors of ferroic materials can be analyzed from their hysteresis which reveal the existence of a strong nonlinearity and phase transition in thermodynamic systems. For example, ferromagnetic materials under an external time-dependent magnetic field e.g. $h(t) = h_0 \sin(\omega t)$, the time-dependent magnetization $m(t)$ is found to lag behind the external field, and m - h hysteresis occurs. Similarly, under the external electric field e.g. $E(t) = E_0 \sin(\omega t)$, the time-dependent polarization $p(t)$ in ferroelectric materials lags behind the field, and p - E hysteresis is also obtained. In ferroelastic materials, under the applied stress σ , the stress-dependent strain ε is found, and ferroelastic hysteresis or ε - σ loop is observed [6]. The p - E , m - h , or ε - σ loops can be numerically studied and simulated by various theoretical models [6–12], to name a few such as the mean-field method based on the Ising model [7, 10, 12] and Heisenberg model [9], and Monte Carlo method based on spin models [8, 11]. After simulating, the ferroic properties can be extracted from their hysteresis loops.

From literatures, by using ferromagnetic notations/language in referring to ferroic behavior, the hysteresis loop area A , coercivity field h_C , remnant magnetization m_r , and the period average magnetization Q are generally investigated. It is usually found that the hysteresis properties depends on the external perturbations, such as the field frequency ω , field amplitude h_0 , and temperature T , and the dynamic phase transition diagram can be obtained from Q [13]. In general, in order to empirically obtain how hysteresis area relates to these perturbations, the power-law scaling is usually performed in many experimental and theoretical studies of ferromagnetic materials [7, 8, 10, 14–16] and ferroelectric materials [17–24]. For instance, the hysteresis area can be written in a form of $A \propto \omega^\alpha h_0^\beta T^\gamma$ where α , β , and γ are exponents to the scaling [16]. After scaling, the exponents can be estimated, and then the power-law dependency on these external factors of the hysteresis area can be predicted. The same way can be applied for remnant magnetization and coercivity.

However, based on the power-law scaling, the obtained exponents are strongly influenced by the considered parameter range. For example, in BaTiO₃ bulk ceramics, above and under the coercive field, the hysteresis area scaling are in the forms $A \propto f^{-0.23} E_0^{0.87}$ and $A \propto f^{-0.36} E_0^{3.64}$ respectively, where f and E_0 are field frequency and field amplitude [22]. In addition, from the A - f relationships, the exponents cannot be predicted in the region close to the turning point (where the scaling function has to change from power-law growth to power-law decay). Consequently, some important hysteresis behavior cannot be fitted (predicted) by power-law scaling. Apart from the power-law scaling, Fourier analysis can also be used to find the relations between the hysteresis area and field parameters, e.g. the ferroelectric hysteresis of the BaTiO₃ bulk ceramic [25].

In this review, to understand how hysteresis behaviors of ferroic materials response to the external perturbations and how to define the dynamic ferroic phase diagram from hysteresis properties in details, fundamental analysis was proposed to study the dynamic ferroic behaviors in microscopic view, and data processing analysis was proposed to link experimental results with external perturbation empirically. In general, data processing analysis is performed to found a connection between the macroscopic phenomena and experimental conditions of ferroic materials. On the other hand, fundamental analysis seeks for the understanding of nature from microscopically inside out. In this review, both fundamental analysis, such as the spin models, the mean-field approach and Monte Carlo

simulation, and the data processing analysis, such as the artificial neural network and Fourier analysis, will be discussed in details in the next section.

2. Methodologies

2.1 Fundamental Analysis

The idea of fundamental analysis is to assume that macroscopic properties of materials are resulted from the interactions in microscopic level. Thus, this method focuses on the microscopic interaction in materials as detailed in the following sections.

2.1.1 Spin Model. A spin model is a mathematical model used widely in studying the dynamic properties of magnetic materials at the microscopic scale. The considered magnetic material consists of many magnetic dipole moments called spins. Under an external magnetic field, the spin Hamiltonian of a system is given as [26]

$$H = - \sum_{\langle ij \rangle} J_{ij} \vec{s}_i \cdot \vec{s}_j + \sum_{ij} K_{ij} \left[\frac{\vec{s}_i \cdot \vec{s}_j}{r_{ij}^3} - \frac{(\vec{s}_i \cdot \vec{r}_{ij})(\vec{s}_j \cdot \vec{r}_{ij})}{r_{ij}^5} \right] + \sum_i (\vec{D}_i \cdot \vec{s}_i)^2 - \sum_i \vec{h}(t) \cdot \vec{s}_i, \quad (1)$$

where J_{ij} represents the exchange interaction between spin vector \vec{s}_i and \vec{s}_j , \vec{D}_i denotes the anisotropic interaction, K_{ij} refers to dipolar interaction strength, and $\vec{h}(t)$ is a time-dependent oscillating external magnetic field. The symbol $\langle ij \rangle$ indicates that sum takes only the first neighbor pairs. By absorbing the unit of s_i into J_{ij} , K_{ij} , D_i and $h(t)$, this gives J_{ij} , K_{ij} , D_i and $h(t)$ to have as a unit of energy. Further, the spin models can be classified into two subgroups – discrete and continuous spin models. The examples of well-known discrete spin models are the Ising model and the Potts model as well as the DIFFOUR model, while the two most widely studied models of continuous spin models are the XY model and the Heisenberg model [27].

Starting with the simplest spin model, i.e. the Ising model, each Ising spin is allowed to have only 2 possible directions on one axis e.g. the z -axis. Therefore, $\vec{s}_i = s_i \hat{z} = \pm 1 \hat{z}$ as s_i can be only ± 1 . Typically, the z -direction is chosen to be the easy axis direction or the applied field direction. If the field is periodic in time and on the z -direction, it is possible to choose $\vec{h}(t) = h_0 \sin(\omega t) \hat{z}$ where h_0 and ω are the field amplitude and field frequency, respectively. For an isotropic case considering only the strongest interaction, it is possible to choose $K_{ij} = D_i = 0$ and $J_{ij} = J$ where J is the ferromagnetic (if $J > 0$) or antiferromagnetic exchange interaction (if $J < 0$). Therefore, from Equation (1), the Ising Hamiltonian can be written as

$$H = -J \sum_{\langle ij \rangle} s_i s_j - \sum_i h(t) s_i, \quad (2)$$

where $h(t) = h_0 \sin(\omega t)$. On the other hand, the Potts model is another discrete spin model, but its spin can take more discrete values, that is, $s_i = 1, 2, 3, \dots, q$ where q is the maximum state a spin can have. Note that the Potts model is equivalent to the Ising model when $q = 2$ [27]. Additionally, an improved version of the Potts model is the DIFFOUR model which is usually used to study the ferroelectric dynamic behaviors which will be discussed in section 2.1.3.

Unlike the discrete-spin models, e.g. the Ising or the Potts model, the XY model provides spin as two-components vector of unit length and can point to any directions on a two-dimensional plane, that is, $\vec{s}_i = (\cos \theta_i, \sin \theta_i)$. Therefore, $\vec{s}_i \cdot \vec{s}_j$ can be replaced by $\cos \theta_{ij}$, where θ_{ij} is an angle between the two spins. It should be noted that although XY spins are two-dimensional vectors, they can also be used in the three-dimensional spatial-structure. The Heisenberg model has a same concept as the XY model, but the spins are three-dimensional unit vectors, and can be represented by two angles of spherical coordinate - ϕ and θ i.e., $\vec{s}_i = (\sin \theta_i \cos \phi_i, \sin \theta_i \sin \phi_i, \cos \theta_i)$ [27]. In this review, both the Ising and Heisenberg models will be discussed through the mean-field approach and Monte Carlo simulation as in the following section.

2.1.2 Mean-Field Theory. The mean-field theory is an analytic method assuming that fluctuations can be neglected, and the magnetic spins align in an effective field created by all surrounding spins and the external field. For the Ising model, within the mean-field framework, the equation of motion for the average magnetization $m(t)$ is given by [28]

$$\tau \frac{dm(t)}{dt} = -m(t) + \tanh \beta \langle E \rangle, \quad (3)$$

where τ represents the microscopic relaxation time, $\beta = 1/k_B T$ where k_B is the Boltzmann's constant, and $\langle E \rangle$ denotes the local field which has the same value overall the system. Further, $\beta \langle E \rangle$ can be written as

$$\beta \langle E \rangle = \frac{z_{nn} J m(t) + h(t)}{k_B T}, \quad (4)$$

where z_{nn} is the coordination number related to the nearest-neighbor isotropic-system (i.e. $z_{nn} = 4, 6, 8$ and 10 for a cubic, simple cubic, body centered cubic and face centered cubic lattice, respectively). Analytically, Eq. (4) can be straightforwardly solved only in simple system, e.g. defect-free, uniform interaction and least surface effect systems. On the other hand, for imperfect structure, solving differential equation using numerical technique, e.g. the fourth order Runge Kutta method, becomes more appropriate to obtain the magnetization as a function of time. Then, from the time-dependent magnetization $m(t)$, the dynamic order parameter (or the so called the period average magnetization) for classifying dynamic hysteresis phase can be defined from $Q = (1/P) \int_0^P m(t) dt$ where $P = 2\pi/\omega$ is the field-period. With this dynamic order parameter, the dynamic phase transition boundaries between the dynamic ferromagnetic phase ($Q \neq 0$) and the dynamic paramagnetic phase ($Q = 0$) can be drawn [13, 29–31]. Specifically, the dynamic critical temperature T_C , which states the phase boundaries, can be defined at the lowest temperature giving $Q = 0$, e.g. see Fig. 1. Therefore, at a fixed field frequency but varying h_0 , pairs of (h_0, T_C) on the dynamic phase boundaries can be obtained. These boundary lines separate a dynamic ferromagnetic phase or asymmetric hysteresis phase (where $Q \neq 0$) from a dynamic paramagnetic phase or symmetric hysteresis phase (where $Q = 0$). For pairs of (h_0, T) lying above the boundary line, a magnetic hysteresis is a symmetric type, but for those lying below the boundary line, a magnetic hysteresis is an asymmetric type. Example of these boundary lines are shown in Fig. 2. Further, with increasing frequencies, the phase boundaries tend to move upward since the phase lag between the magnetization and the external magnetic field is enhanced. Therefore, the asymmetric-hysteresis behavior is

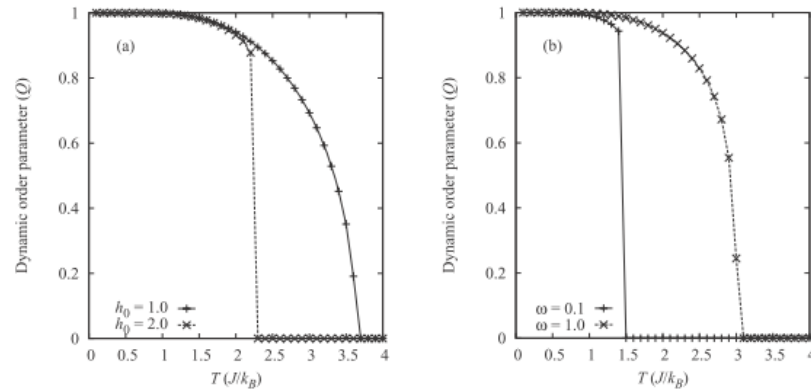


Figure 1. The dynamic order parameter profiles of the mean-field Ising hysteresis extracted at (a) $\omega = 0.5 \tau^{-1}$ (presenting a continuous transition at $h_0 = 1.0 J$ but a discontinuous transition at $h_0 = 2.0 J$) and (b) $h_0 = 1.0 J$ (presenting a continuous transition at $\omega = 1.0 \tau^{-1}$ but a discontinuous transitions at $\omega = 0.1 \tau^{-1}$).

more outstanding, since the magnetization has less time to follow the oscillating field. Further, it is found that the change in Q from finite to zero values (from dynamic ferromagnetic phase to dynamic paramagnetic phase) can be either continuous transition or discontinuous transitions, depending on field amplitudes and field frequencies, as shown in Fig. 1.

For Heisenberg model, the mean-field equation can be proposed using kinetic Bethe-Peierls approximation (KBPA) [10, 32, 33]. For instance, for ferromagnetic films with

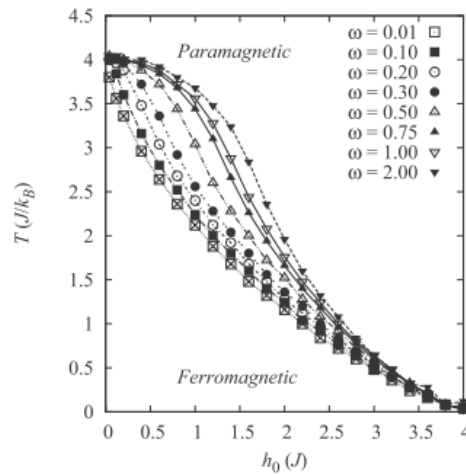


Figure 2. The dynamic phase diagram of the two-dimensional Ising-hysteresis extracted from mean-field analysis. The frequency ω is in a unit of τ^{-1} and lines are used for visual aids.

the simple cubic structure and N Heisenberg spins in three-dimension [9], the mean-field equation of average magnetization can be written as [34]

$$\tau \frac{d\bar{m}(t)}{dt} = -\bar{m}(t) + \frac{\sum_i \bar{s}_i e^{-E_i/k_B T}}{\sum_i e^{-E_i/k_B T}}, \quad (5)$$

In Eq. (5), E_i refers to the energy of the i^{th} spin. If only exchange interaction and anisotropic energy are taken into account, E_i could take a form [9]

$$E_i = -\bar{s}_i \cdot [z_{nn}(m_x \hat{x} + m_y \hat{y} + m_z \hat{z}) + (K/a)(\bar{s}_i \cdot \hat{u}_i) \hat{u}_i + \bar{h}(t)/a], \quad (6)$$

where K is the anisotropy constant which easy axis is parallel to \hat{u}_i and $a = \lambda J$ where λ is the mean-field coefficient. Note that $a = 1$ can be used as unit of energy. In addition, \hat{u}_i and $\bar{h}(t)$ are all along z -axis, that is $\hat{u}_i = \hat{z}$. Further, if $K = 0$ and $\bar{s}_i = \pm 1$, Eq. (6) becomes a scalar equation of motion [10, 12]. In addition to that of the Ising model, the period average magnetizations should be investigated both along z - and x -axes, i.e. $Q_z = (\omega/2\pi) \oint m_z(t) dt$ and $Q_x = (\omega/2\pi) \oint m_x dt$, along with the hysteresis area, i.e. $A_i = (\omega/2\pi) \oint m_i(t) dh$ ($i = x, y, z$). It was found that m_z-h and $Q-T$ loops for the Heisenberg model are different from those for the Ising model due to more degree of freedom of the spin directions [9].

2.1.3 Monte Carlo Simulation. Although the mean-field method can predict magnetic phase transition and explain magnetic behaviors near the critical temperature T_C , it generally overestimates T_C and reports critical-exponent values that do not depend on system dimensionality [35]. These are the weak points of the mean-field analysis caused by neglecting important fluctuation near the phase transition. On the other hand, Monte Carlo simulation is one of the well-known sophisticate methods in studying statistical physical problem, including phase transition and critical phenomena topics. The basic concept behind Monte Carlo simulation is to use stochastic process (e.g. Boltzmann's probability and random thermal fluctuation) to take the system from one state μ to another possible state ν . The system can then pass through series of states with well-defined set of probabilities at time t , i.e. $\{p_\mu(t)\}$. The state evolution is governed by the master equation [27]

$$\frac{dp_\mu(t)}{dt} = \sum_\nu [p_\nu(t)R(\nu \rightarrow \mu) - p_\mu(t)R(\mu \rightarrow \nu)], \quad (7)$$

where $R(\mu \rightarrow \nu)$ is the transition rate for the probability $p_\mu(t) = (1/Z)e^{-\beta E_\mu}$, $Z = \sum_\mu e^{-\beta E_\mu}$, E_μ denotes the energy of state μ , and $\beta = 1/k_B T$. Currently, the commonly used algorithms in Monte Carlo simulation for spin models can be divided into spin-flip and cluster-flip algorithms.

In spin-flip algorithm, a spin is chosen at random and updated to a new spin (different value), and the unit is accepted with the Metropolis probability [36]

$$w_M(\mu \rightarrow \nu) = \begin{cases} e^{-\beta \Delta E}; & \Delta E > 0 \\ 1 & ; \text{otherwise} \end{cases}, \quad (8)$$

or the Glauber probability [27]

$$w_G(\mu \rightarrow \nu) = \begin{cases} (1 + e^{\beta \Delta E})^{-1}; & \Delta E > 0 \\ 1 & ; \text{otherwise} \end{cases}. \quad (9)$$

In Eqs. (8) and (9), ΔE is the energy difference due to the spin update (the spin flip). Between these 2 algorithms, the Metropolis algorithm is more efficient at high temperature but the Glauber algorithm is more effective at low temperature. However, due to less computational effort in each turn, the Metropolis is more commonly used than the Glauber in studying critical behavior of spin model. Further, the simulation time unit is usually termed as 1 Monte Carlo Step per site or 1 MCS, which equals to N spins update (either successful or unsuccessful) and N refers to total number of spins in the system.

Although the spin-flip algorithm is easy to implement, it has a disadvantage in guiding the system towards equilibrium state at temperatures close to the critical point. Therefore, the properties extracted from these temperatures in the critical region tend to suffer from large statistical error due to the large correlation time among successive states. To overcome the problem, the cluster-flip algorithms, such as Swendsen-Wang (SW) [37] and Wolff [38] algorithms, were proposed. The central idea is to make the clusters of spins and flip all spins in each cluster in one move, rather than trying to switch spin one by one. Consequently, this enhances the state updating towards equilibration, lessens the correlation time, and improves the statistical error. However, the cluster-flip algorithms are somewhat difficult to be applied for anisotropic system. Further, since the clusters of spins vary in sizes and strongly depend on system temperature and internal-interaction, it is unlikely to define universal time-unit for the simulation. Therefore, most Monte Carlo studies of dynamic hysteresis behaviors tend to use the spin-flip algorithm as it is more convenient.

Similar to the mean-field analysis, the dynamic phase transition boundaries can also be investigated using the Monte Carlo simulation. For instance, Fig. 3 shows the dynamic phase transition diagram obtained from performing Monte Carlo simulation on two-dimensional Ising model. The results are found to qualitatively agree well with the mean-field approach,

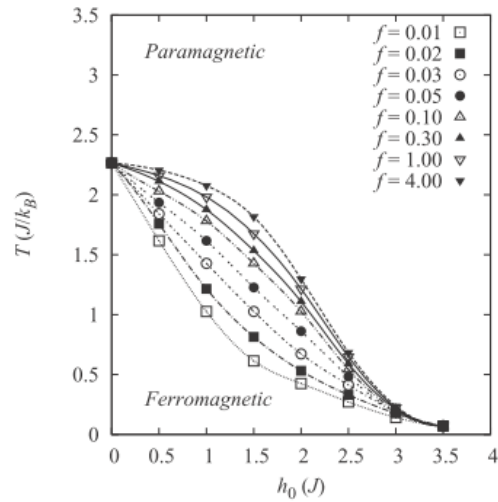


Figure 3. The dynamic phase diagram of the two-dimensional Ising-hysteresis extracted from Monte Carlo simulation. The frequency f is in a unit of mcs^{-1} and lines are used for visual aids.

that is, with increasing the frequencies, the phase boundaries tend to move upward. This confirms that the dynamic phase transition behavior is universal in general and does not depend on the techniques used in the investigation. Nevertheless, it is worth to emphasize that it is not possible to directly compare the results (the boundary lines) of these 2 techniques quantitatively. This is as by nature of mean-field method, any fluctuations are discarded, but the Monte Carlo takes the fluctuations very much into account. Henceforth, their quantitative results are different both in values and physical meaning especially in the critical region.

Apart from the ferromagnetic subject, the basic idea of spin model can also be applied to study the dynamic hysteresis behaviors of ferroelectric materials. In ferroelectric spin systems, p - E loops can be obtained using Monte Carlo simulation on the DIFFOUR model. In many previous works, the DIFFOUR model was successfully used to investigate the dynamic ferroelectric hysteresis [39–42]. For example, ferroelectric hysteresis properties in thin films were investigated using the DIFFOUR model with the Metropolis algorithm [41]. It was found that their hysteresis properties, such as the hysteresis area, remnant polarization and coercivity field, depend on the film-thickness, frequency and amplitude of the field. Moreover, the DIFFOUR model can be considered in a special material, such as acceptor-doped ferroelectric material [42]. The obtained hysteresis profiles qualitatively agreed well with experimental results. The concepts of the DIFFOUR model can be described as the following.

Based on the DIFFOUR model, the Hamiltonian can be written as [43, 44]

$$H = \sum_i \left(\frac{P_0^2}{2m} - \frac{a}{2}u_i^2 + \frac{b}{2}u_i^4 \right) - \sum_{\langle ij \rangle} U_{ij} \vec{u}_i \cdot \vec{u}_j - \sum_i \vec{E}(t) \cdot \vec{u}_i, \quad (10)$$

where $P_0^2/2m$ is the kinetic energy, \vec{u}_i is the ferroelectric dipole (polarization) at site i , a and b are the double-well potential parameters, $\langle ij \rangle$ means that only nearest neighbors pairs are taken into the sum, U_{ij} refers to the ferroelectric interaction and $\vec{E}(t) = E_0 \sin(2\pi ft)\hat{z}$ is the time-dependent electric-field along one axis, e.g. the z -axis. In Eq. (10), the first summation is due to the Landau free energy, the second summation represents the electrical dipole-dipole energy, and the last summation is the external electric field energy. In many previous works, a and b were set as constants with the condition $a/b < 1$ [40, 45–47], such as $a/b = 0.1$ [40, 47] or $a/b = 0.5$ [45, 46]. This is to satisfy the Landau phase transition between ferroelectric and paraelectric phase. In the Landau theory, a is proportional to temperature away from the critical point, that is $a \propto (T_c - T)$. Therefore, close to the critical point, or $ab \ll 1$, the Landau theory gives a solution of $u_i^2 = a/b$ under the absence of external electric field which is found to agree with mean-field solutions [48]. As a result, although the ratio ab changes, but as long as it is small enough, the qualitative ferroelectric behavior close to the critical point should remain the same.

In performing Monte Carlo simulation using the DIFFOUR model, if the considered ferroelectric behavior is mainly due to the dipole switching, e.g. the behavior close to the critical point, $|u_i|$ may be assumed temperature independent. Therefore, at a fixed temperature simulation, $\sum_i \left(\frac{P_0^2}{2m} - \frac{a}{2}u_i^2 + \frac{b}{2}u_i^4 \right)$ may be assumed as a constant and can be assigned as new energy reference. In this case, Eq. (10) reduces to

$$H = - \sum_{\langle ij \rangle} U_{ij} \hat{u}_i \cdot \hat{u}_j - E(t) \sum_i u_{iz}, \quad (11)$$

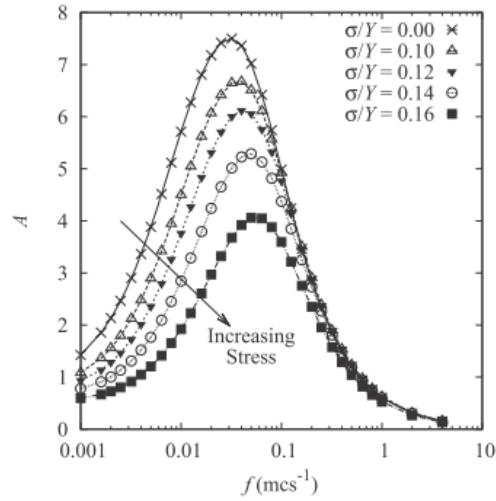


Figure 4. Stress dependence of the hysteresis areas as a function of the electric field frequency obtained from Monte Carlo simulation on the DIFFOUR model. Lines are used for visual aids.

where \hat{u}_i is a unit vector referring to one of the possible ferroelectric dipole directions (e.g. 14 directions from rhombohedral and tetragonal structures), u_{iz} is the dipole' s z -component at site i . For directional uniformity, $U_{ij} = U$ may be treated as a constant [40, 45–47]. However, under some circumstances, U_{ij} could be directional dependent e.g. in anisotropic material or under the application of external perturbations. For instance, with an application of uniaxial stresses perturbation σ/Y , i.e. the stress to Young's modulus ratio, the ferroelectric interaction U_{ij} becomes directional dependent and is a function of σ/Y [49]. Accordingly, in such the case, ferroelectric hysteresis area A depends on the stress ratio σ/Y [50]. For example, with increasing stresses, it was found that the hysteresis area decreases, and the maximum area shifts to higher frequency, as shown in Fig. 4. This is because, the stress suppresses the growth of average polarization along the applied stress direction, and hence p_r and A . Further, it also lessens ferroelectric interaction, so the maximum phase lag (where A is maximum), shifts to higher frequencies with increasing stresses [50].

2.2 Data Processing Analysis

Although fundamental analysis is an appropriate method used to understand the nature behaviors of materials, but sometimes it is too difficult to use this method due to the complexity of materials. Data processing analysis is a very straightforward way to establish the relationship between input and output parameters without the need to acquire the fundamental knowledge. Mostly it is used for designing extensive database for specific ranges of input for easy and quick prediction of the output. Although it has been limited to use outside the original input range, due to nature of empirical recognition, it is worthwhile in enhancing technological development in designing applications used in known/specific environments. In this review, the 'learn by example' Artificial Neural Network and the 'harmonic recognition' Fourier transformation are presented as examples.

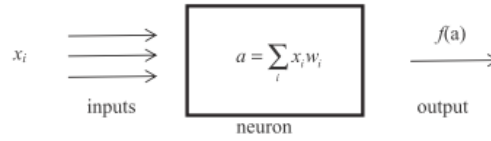


Figure 5. Schematic diagram displaying the input signals, the input-weighted-sum and the output signal of a neuron in ANN modeling.

2.2.1 Artificial Neural Network. The Artificial Neural Network (ANN) is a computer model consisting of a number of processing elements or ‘artificial neurons’ inspired by the real human neurons in the brain. In the human brain, when a neuron receives a strong enough signal, it is activated and emits the signal to adjacent neurons, and the signal is linked to a recognized perception taken from the pool of experiences. In the same manner, each artificial neuron behaves as a processing unit which receives inputs (usually more than one) and transforms them to input-weighted-sum $a = \sum_{\text{all inputs}} x_i w_i$, where x_i is an input signal and w_i is a signal weight. To compute the output, an activation function f is applied on a , then the output $f(a)$ is obtained as illustrated in Fig. 5. One of the most commonly used activation functions takes form of

$$f(x) = \frac{1}{1 + e^{-cx}}, \tag{12}$$

where $x = a$ and c is a positive scaling constant.

In performing ANN modeling, artificial neurons are organized in layers (see Fig. 6), where the first layer on the left hand side is the input layer. Input data are fed to the network through this layer. Outputs from ANN are obtained from the output layer on the right hand side. The layers between input and output are called the hidden layers. There may be one or more hidden layers between the input and output layers. Neurons in each layer are connected together (indicated by a lines connecting between neurons). The strength of the connection is indicated by signal weight (w_i). In Fig. 6, the field frequency, field amplitude, or temperatures are provided in the input layer, and the corresponding hysteresis area is

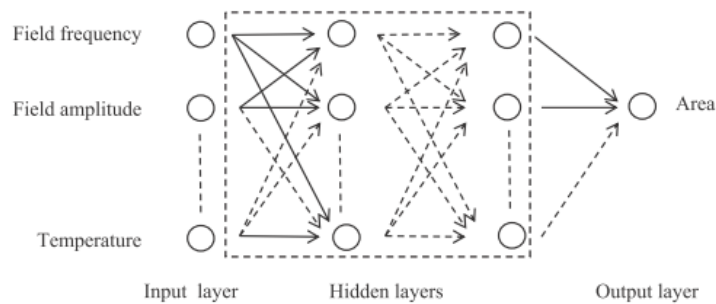


Figure 6. An example of schematic diagram for ANN modeling of ferroelectric hysteresis area.

obtained from the output layer. However, if preferred, there could be more than one output in the output layer, such as hysteresis area, remnant magnetization, coercive field, and etc.

During the ANN processing, the signal weights w_i are adjusted to minimize the error between the network outputs and desired outputs. The weight adjustment process is called 'training' which is governed by the learning algorithm. One of most well-known learning algorithms is the Back Propagation (BP) algorithm [51, 52]. The idea of the BP algorithm can be described as the following. The training begins with assigning small random number to all signal weights. Then two-stages calculations are performed. Firstly, in the 'forward pass' input data are presented to the network, and then output from each neurons are calculated using input-weighted-sum a and Eq. (12) to obtain the final outputs in the output layer. These outputs are then compared with the actual outputs, and the deviation or error are determined. Secondly, the 'backward pass' is performed by adjusting all signal weights in order to minimize the error. These two-stages calculations are repeated with the new set of input-output examples until the stopping criterion is met, and the weights are kept for ANN prediction.

The ANN model has been efficiently applied to many works in physics and materials science [16, 51, 53–56], manufacturing [57, 58] and business [59, 60]. For example, an ANN model was used in modeling ceramics-powder preparation in obtaining the pure perovskite phase [54]. It was also used to found the complex relation between ferroelectric hysteresis properties and external electric field parameters [56], and between ferromagnetic hysteresis behavior and external magnetic field perturbation [16]. An example of how accurate the ANN is in hysteresis modeling can be found in Fig. 7, where the predicted and the real hysteresis areas were found to agree well over the considered parameter ranges. As can be seen, this truly reflects the advantages of using ANN modeling as the dynamic hysteresis behavior can be predicted without the comprehension of how dynamic hysteresis behaviors depend on the applied perturbation and complex internal interaction in the system.

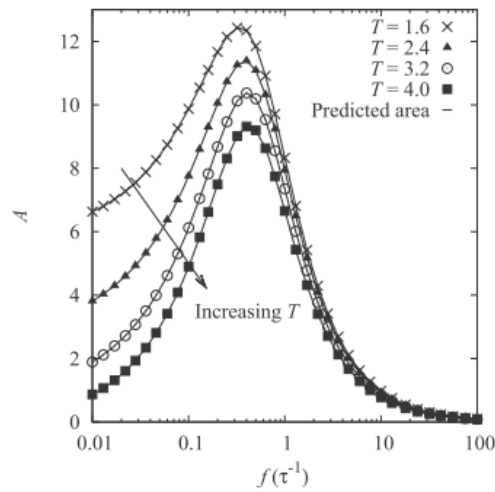


Figure 7. Comparison of the predicted hysteresis area from ANN (solid lines) and the actual hysteresis area taken from mean-field analysis on two-dimensional Ising hysteresis at $h_0 = 3.25 J$.

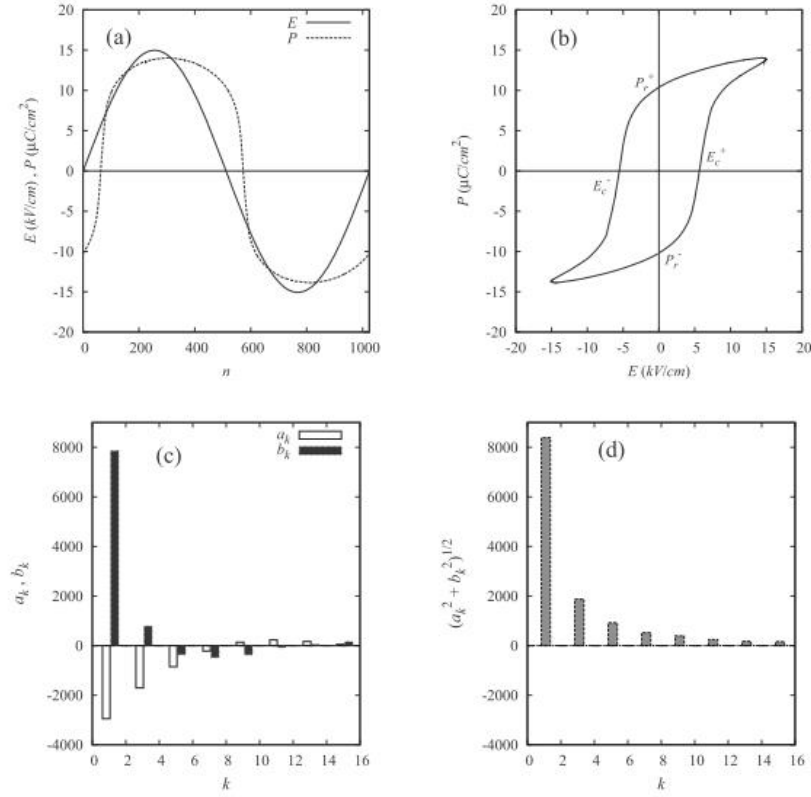


Figure 8. The hysteresis results of the bulk BaTiO₃, measured at $E_0 = 10$ kV/cm, $f = 10$ Hz and room temperature (25°C), which are (a) the electric field and polarization as a function of data points and (b) the p - E hysteresis loop, and their Fourier results which are (c) the k^{th} harmonic amplitudes of real and imaginary parts and (d) the associated amplitude spectrum.

2.2.2 Fourier Transformation. In Fourier transformation, any periodic function in time domain $f(t)$ can be expressed as the sum of sine and cosine series, i.e.

$$f(t) = \frac{1}{2}a_0 + \sum_i a_i \cos(\omega_i t) + \sum_i b_i \sin(\omega_i t); \quad i = 1, 2, 3, \dots \quad (13)$$

where a_0 , a_i and b_i are Fourier coefficients, ω_i is the i^{th} -order frequency, and t is time. Fourier transformation is an alternative method that can be used to model the dynamic hysteresis behaviors. However, since hysteresis data are discretely measured at a time interval δt , the time domain parameter t has to be represented by the data-point domain n . For instance, by taking hysteresis of BaTiO₃ bulk ceramics as an application [25], the electric field and polarization as a function of data-point can be shown in Fig. 8(a), while the original field dependence of polarization, or p - E hysteresis loop, is illustrated in Fig. 8(b). In order to

change the data from data-point domain n to the frequency domain k , Fourier transformation is considered as the following equation [25, 61, 62]

$$F(k) = \sum_{n=0}^{N-1} f(n)e^{-i2\pi nk/N}, \quad (14)$$

which can be rewritten as

$$F(k) = \sum_{n=0}^{N-1} f(n) \cos(2\pi nk/N) - i \sum_{n=0}^{N-1} f(n) \sin(2\pi nk/N) = a_k - ib_k, \quad (15)$$

where N is the number of data points in one field period, a_k and b_k are the Fourier coefficients or the amplitudes of k^{th} harmonic of real and imaginary parts, respectively. Then, by applying Eq. (15) to ferroelectric hysteresis of BaTiO₃ bulk ceramics measured at $E_0 = 10$ kV/cm, $f = 10$ Hz and room temperature (25°C) [25], the k^{th} harmonic amplitudes of real and imaginary parts of the polarization signal can be shown in Fig. 8(c). As can be seen, all even-harmonics are small due to the almost symmetric behavior of the hysteresis loop. Therefore even-harmonics can be ignored, while the odd-harmonics are prominent, especially the first harmonic as shown in Fig. 8(d). As a result, the hysteresis area can be calculated from [25]

$$A = -\frac{2\pi}{N} E_0 a_1, \quad (16)$$

where a_1 is the first-harmonic amplitude of the real part and E_0 represents the field amplitude. It was also found that the positive and negative remnant polarizations depend on all odd-harmonic of real parts as

$$p_r^\pm = \mp \frac{2}{N} \sum_{n=1}^{N/2} a_n. \quad (17)$$

In addition, the positive and negative coercive field can be computed from the first-harmonic amplitude of both real and imaginary parts as

$$E_c^\pm = \pm E_0 \sin[\tan^{-1}(a_1/b_1)]. \quad (18)$$

To confirm their validities, the hysteresis area from Eq. (16), the remnant polarizations from Eq. (17) and coercive fields from Eq. (18) were compared with those measured from experiment, and were found to agree very well as shown in Table 1.

Table 1
Comparison of ferroelectric hysteresis properties obtained from the Fourier prediction and real measurement

Observables	Fourier prediction	Real measurement
A (mCV/cm ³)	133.6468	133.5459
$\frac{p_r^+ - p_r^-}{2}$ ($\mu\text{C}/\text{cm}^2$)	8.1887	8.1887
$\frac{E_c^+ - E_c^-}{2}$ (kV/cm)	3.4367	3.4594

In fact, these hysteresis properties can be directly extracted from the original hysteresis. For instance, the hysteresis area can be calculated by performing the numerical integration methods e.g. trapezoidal or Simpsons methods. However, due to the electronic noise or poor experimental set up, the p - E loops obtained from the experiment may be distorted, asymmetric, or unexpectedly shifted along p -axis or E -axis. These random or unwanted noises distort the hysteresis loop from its ideal shape and hence hysteresis area. Consequently, this may concealed some important fundamental phenomena and may prohibit unbiased link between the true hysteresis properties and the external perturbations. Therefore, the Fourier transformation can be used to ease these problems.

3. Summary

In this review, ferroic hysteresis modeling was categorized in terms of both fundamental and data processing analysis. Several approaches for fundamental investigation, such as mean-field analysis and Monte Carlo simulation, and data analysis investigation, such as Artificial Neural Network and Fourier analysis, were detailed. Examples of how to use these approaches on ferromagnetic and ferroelectric systems were reported with evidences of applicability. However, to enhance the ferroic understanding from individual ferroic material to multi-ferroic systems, in future work, the coupling effect between different ferroic properties and field perturbations, such as magnetostrictive effect, or electrostrictive effect, shall be elaborately considered.

Acknowledgment

This work was supported by the Graduated School, Faculty of Science, Chiang Mai University, National Electronics and Computer Technology Center, National Science and Technology Development Agency, and the Industry/University Cooperative Research Center (I/UCRC) in HDD Component, the Faculty of Engineering, Khon Kaen University.

References

1. V. K. Wadhawan, *Smart Structures: Blurring the Distinction Between the Living and the Nonliving*. New York: Oxford University Press; 2007.
2. J. F. Scott, *Ferroelectric Memories*. Berlin: Springer-Verlag; 2002.
3. J. H. Judy, Past, present, and future of perpendicular magnetic recording. *J. Magn. Magn. Mater.* **235**, 235–240 (2001).
4. J. V. Humbeeck, Non-medical applications of shape-memory alloys. *Mater. Sci. Eng. A* **273–275**, 134–147 (1999).
5. R. D. James and K. F. Hane, Martensitic transformations and shape-memory materials. *Acta Mater.* **48**, 197–222 (2000).
6. M. Kamlah, Ferroelectric and ferroelastic piezoceramics modeling of electromechanical hysteresis phenomena. *Continuum Mech. Thermodyn.* **13**, 219–268 (2001).
7. M. Acharyya and B. K. Chakrabarti, Response of Ising system to oscillating and pulsed fields: Hysteresis, ac, and pulse susceptibility. *Phys. Rev. B.* **52**, 6550–6568 (1995).
8. B. K. Chakrabarti, Dynamic transitions and hysteresis. *Rev. Mod. Phys.* **71**, 847–859 (1999).
9. Z. Huang, Z. Chen, F. Zhang, and Y. Du, Dynamic phase transition in the Heisenberg model under a time-dependent oscillating field. *Phys. Lett. A.* **338**, 485–493 (2005).
10. C. N. Luse and A. Zangwill, Discontinuous scaling of hysteresis losses. *Phys. Rev. E.* **50**, 224–226 (1994).
11. M. Rao, H. R. Krishnamurthy, and R. Pandit, Magnetic hysteresis in two model spin systems. *Phys. Rev. B.* **42**, 856–884 (1990).

12. T. Tome and M. J. d. Oliveira, Dynamic phase transition in the kinetic Ising model under a time-dependent oscillating field. *Phys. Rev. A* **41**, 4251–4254 (1990).
13. A. Punya, R. Yimnirun, P. Laoratanakul, and Y. Laosiritaworn, Frequency dependence of the Ising-hysteresis phase- diagram: Mean-field analysis. *Physica B* **405**, 3482–3488 (2010).
14. J.-S. Suen, M. H. Lee, G. Teeter, and J. L. Erskine, Magnetic hysteresis dynamics of thin Co films on Cu(001). *Phys. Rev. B* **59**, 4249–4259 (1999).
15. W. Y. Lee, B.-C. Choi, Y. B. Xu, and J. A. C. Bland, Magnetization reversal dynamics in epitaxial Fe/GaAs(001) thin films. *Phys. Rev. B* **60**, 10216–10221 (1999).
16. W. Laosiritaworn and Y. Laosiritaworn, Artificial neural network modeling of mean-field Ising hysteresis. *IEEE Trans. Magn.* **45**, 2644–2647 (2009).
17. R. Yimnirun, S. Ananta, Y. Laosiritaworn, A. Ngamjarujana, and S. Wongsanmai, Scaling behavior of dynamic ferroelectric hysteresis in soft PZT ceramic: Stress dependence. *Ferroelectr.* **358**, 3–11 (2007).
18. R. Yimnirun, Y. Laosiritaworn, S. Wongsanmai, and S. Ananta, Scaling behavior of dynamic hysteresis in soft lead zirconate titanate bulk ceramics. *Appl. Phys. Lett.* **89**, 162901 (2006).
19. R. Yimnirun, N. Wongdamnern, N. Triamnak, M. Unruan, A. Ngamjarujana, S. Ananta, and Y. Laosiritaworn, Stress dependence and scaling of subcoercive field dynamic hysteresis in $0.5\text{Pb}(\text{Zr}_{1/2}\text{Ti}_{1/2})\text{O}_3$ - $0.5\text{Pb}(\text{Zn}_{1/3}\text{Nb}_{2/3})\text{O}_3$ ceramic. *J. Appl. Phys.* **104**, 104103 (2008).
20. R. Yimnirun, R. Wongmaneeerung, S. Wongsanmai, A. Ngamjarujana, S. Ananta, and Y. Laosiritaworn, Dynamic hysteresis and scaling behavior of hard lead zirconate titanate bulk ceramics. *Appl. Phys. Lett.* **90**, 112908 (2007).
21. R. Yimnirun, S. Wongsanmai, S. Ananta, and Y. Laosiritaworn, Stress-dependent scaling behavior of dynamic hysteresis in bulk soft ferroelectric ceramic. *Appl. Phys. Lett.* **89**, 242901 (2006).
22. N. Wongdamnern, A. Ngamjarujana, S. Ananta, Y. Laosiritaworn, and R. Yimnirun, Dynamic hysteresis scaling in BaTiO_3 bulk ceramics. *Key Eng. Mater.* **421–422**, 399–402 (2010).
23. N. Wongdamnern, A. Ngamjarujana, Y. Laosiritaworn, S. Ananta, and R. Yimnirun, Dynamic ferroelectric hysteresis scaling of BaTiO_3 single crystals. *J. Appl. Phys.* **105**, 044109 (2009).
24. N. Wongdamnern, N. Triamnak, Y. Laosiritaworn, and R. Yimnirun, Stress-dependent scaling behavior of sub-coercive field dynamic hysteresis in $\text{Pb}(\text{Zr}_{1/2}\text{Ti}_{1/2})\text{O}_3$ - $\text{Pb}(\text{Zn}_{1/3}\text{Nb}_{2/3})\text{O}_3$ ceramic systems. *Ferroelectr.* **384**, 1–9 (2009).
25. K. Kanchiang, R. Yimnirun, N. Wongdamnern, A. Ngamjarujana, and Y. Laosiritaworn, Harmonic analysis of dynamics hysteresis response of BaTiO_3 bulk ceramics. *Ferroelectr.* **401**, 123–128 (2010).
26. D. P. Landau and K. Binder, *A Guide to Monte Carlo Simulations in Statistical Physics*. 2 ed., New York: Cambridge University Press; 2000.
27. M. E. J. Newman and G. T. Barkema, *Monte Carlo Methods in Statistical Physics*. Oxford: Oxford University Press; 1999.
28. M. Suzuki and R. Kubo, Dynamics of the Ising model near the critical point. I. *J. Phys. Soc. Jpn.* **24**, 51–60 (1968).
29. M. Acharyya, Nonequilibrium phase transition in the kinetic Ising model: Critical slowing down and the specific-heat singularity. *Phys. Rev. E* **56**, 2407–2411 (1997).
30. M. Acharyya, Nonequilibrium phase transition in the kinetic Ising model: Is the transition point the maximum lossy point? *Phys. Rev. E* **58**, 179–186 (1998).
31. Y. Laosiritaworn, A. Punya, S. Ananta, and R. Yimnirun, Mean-field analysis of the Ising hysteresis relaxation time. *Chiang Mai J. Sci.* **36**, 263–275 (2009).
32. C. N. Luse and A. Zangwill, Dynamic hysteresis of two-dimensional magnetic islands with uniaxial anisotropy. *J. Appl. Phys.* **79**, 4942–4944 (1996).
33. Y. Saito and H. M. Krumbhaar, Diffusion and relaxation kinetics in stochastic models for crystal growth. *J. Chem. Phys.* **70**, 1078–1095 (1979).
34. R. H. Kodama and A. E. Berkowitz, Atomic-scale magnetic modeling of oxide nanoparticles. *Phys. Rev. B* **59**, 6321–6336 (1999).
35. N. J. Giordano, *Computational physics*. New Jersey: Prentice Hall; 1997.

36. N. Metropolis, A. W. Rosenbluth, M. N. Rosenbluth, and A. H. Teller, Equation of state calculations by fast computing machines. *J. Chem. Phys.* **21**, 1807–1092 (1953).
37. R. H. Swenden and J.-S. Wang, Nonuniversal critical dynamics in Monte Carlo simulations. *Phys. Rev. Lett.* **58**, 86–88 (1987).
38. U. Wolff, Collective monte carlo updating for spin systems. *Phys. Rev. Lett.* **62**, 361–364 (1989).
39. J.-M. Liu, Q. C. Li, W. M. Wang, X. Y. Chen, G. H. Cao, X. H. Liu, and Z. G. Liu, Scaling of dynamic hysteresis in ferroelectric spin system. *J. Phys. Condens. Matter* **13**, L153 (2001).
40. J.-M. Liu, W. M. Wang, Z. G. Liu, H. L. Chan, and C. L. Choy, Dynamic hysteresis in ferroelectric systems: experiment and Monte Carlo simulation. *Appl. Phys. A* **75**, 507–514 (2002).
41. Y. Laosiritaworn, Monte Carlo investigation of ferroelectric properties in thin films. *Key Eng. Mater.* **421–422**, 177–181 (2010).
42. S. Sucharitakul, R. Yimnirun, and Y. Laosiritaworn, Accetor-doped ferroelectric modeling via Monte Carlo Simulation. *Key Eng. Mater.* **421–422**, 231–234 (2010).
43. T. Janssen and J. A. Tjon, One-dimension model for a crystal with displacive modulation. *Phys. Rev. B* **24**, 2245–2248 (1981).
44. J.-M. Liu, Q. C. Li, W. M. Wang, X. Y. Chen, G. H. Cao, X. H. Liu, and Z. G. Liu, Scaling of dynamic hysteresis in ferroelectric spin system. *J. Phys. Condens. Matter* **13**, L153–L161 (2001).
45. X. S. Gao, J.-M. Liu, X. Y. Chen, and Z. G. Liu, Monte Carlo approach to phase transitions in ferroelectromagnets. *J. Appl. Phys.* **88**, 4250–4256 (2000).
46. X. S. Gao, J.-M. Liu, Q. C. Li, and Z. G. Liu, A Monte-Carlo study of magnetoelectric coupling system. *Ferroelectr.* **252**, 69–77 (2001).
47. J.-M. Liu, K. F. Wang, Y. Wang, Q. C. Li, and X. S. Gao, Magnetoelectric coupling in ferroelectromagnets with antiferroelectric and antiferromagnetic orders. *Comput. Mater. Sci.* **30**, 389–396 (2004).
48. R. Bowley and M. M. Sanchez, Introductory statistical mechanics. Oxford: Clarendon Press; 1999.
49. S. J. Mitchell and D. P. Landau, Phase separation in a compressible 2D Ising model. *Phys. Rev. Lett.* **97**, 025701 (2006).
50. Y. Laosiritaworn, S. Ananta, J. Poulter, and R. Yimnirun, Monte Carlo investigation of hysteresis properties in ferroelectric thin-films under the effect of uniaxial stresses. *Ceram. Int.* **35**, 181–184 (2009).
51. C. A. O. Nascimento, R. Giudici, and R. Guardani, Neutral network based approach for optimization of industrial chemical processes. *Comput. Chem. Eng.* **24**, 2303–2314 (2000).
52. D. Rumelhart and J. McClelland, Parallel Distributed Processing. Cambridge: MIT Press; 1986.
53. W. Laosiritaworn and N. Chotchaithanakorn, Artificial neural networks parameters optimization with design of experiments: An application in ferromagnetic materials modeling. *Chiang Mai J. Sci.* **36**, 83–91 (2009).
54. W. Laosiritaworn, O. Khamman, S. Ananta, R. Yimnirun, and Y. Laosiritaworn, Artificial neural network model of ceramics power preparation: Application to NiNb_2O_6 . *Ceram. Int.* **34**, 809–812 (2008).
55. W. Laosiritaworn, O. Khamman, S. Ananta, R. Yimnirun, and Y. Laosiritaworn, Artificial neural network modeling of ceramics powder preparation: Application to NiNb_2O_6 . *Ceram. Int.* **34**, 809–812 (2008).
56. W. Laosiritaworn, R. Yimnirun, and Y. Laosiritaworn, Artificial neural network modeling of ferroelectric hysteresis: An application to soft lead zirconate titanate ceramics. *Key Eng. Mater.* **421–422**, 432–435 (2010).
57. G. J. Udo, Neural neural applications in manufacturing processes. *Comput. Ind. Eng.* **23**, 97–100 (1992).
58. H. C. Zhang and S. H. Huang, Applications of neural networks in manufacturing: A state-of-the-art survey. *Int. J. Prod. Res.* **33**, 705–728 (1995).
59. A. Vellido, P. J. G. Lisboa, and J. Vaughan, Neural networks in Business: A survey of applications (1992–1998). *Expert. Syst. Appl.* **17**, 51–70 (1999).

60. B. K. Wong, V. S. Lai, and J. Lam, A bibliography of neural network business applications research: 1994–1998. *Comput. Oper. Res.* **27**, 1045–1076 (2000).
61. G. Goev, V. Masheva, and M. Mikhov, Fourier analysis of AC hysteresis loops. *IEEE Trans. Magn.* **39**, 1993–1996 (2003).
62. S. Srilomsak, W. A. Schulze, S. M. Pilgrim, and F. A. Williams, Harmonic analysis of polarization hysteresis of aged PZTs. *J. Am. Ceram. Soc.* **88**, 2121–2125 (2005).

Monte Carlo Investigation of Defect-Driven Ferroelectric Phase-Transition in Two Dimensional Defected Film

S. SRINOI^{1,2} AND Y. LAOSIRITAWORN^{1,2,*}

¹Center of Excellence in Materials Science, Faculty of Science, Chiang Mai University, Chiang Mai 50200, Thailand

²Department of Physics and Materials Science, Faculty of Science, Chiang Mai University, Chiang Mai 50200, Thailand

In this work, the hysteresis loops of ferroelectric film with defects were investigated with Monte Carlo simulation and the modified Heisenberg model (discrete vector model) with DIFFOUR type interaction. The effect of localized vacancy defects on the electrical properties of ferroelectric film was studied. The defected ferroelectric film was simulated on the two-dimensional lattice with periodic boundary conditions. From results, at a given electric field, the hysteresis loop area was found to depend on the defect concentration of system. The higher defect concentration, the smaller hysteresis loop was obtained, which resulted from weaker ferroelectric interaction.

Keywords Heisenberg model; DIFFOUR interaction; hysteresis loop; Monte Carlo simulation

1. Introduction

Ferroelectrics are useful materials and have been widely used as parts in various electronic devices such as capacitor, sensor, actuator, and nonvolatile memory [1]. Due to the high-speed memory, the ferroelectric thin-film devices have been developed extensively. The responses of ferroelectric thin film to external field electric were investigated in detail to design more efficient devices [2, 3]. Typically, ferroelectric material undergoes a succession of phase-transitions from high-structural-symmetry paraelectric phase at high temperatures to low-structural-symmetry ferroelectric phase at low temperatures. Although many defect-free systems had been investigated and reported [4–7], the deep understanding in relationship between structural symmetry and the phase transition from paraelectric to ferroelectric (and vice versa) is still incomplete material intrinsic defects are taken into account. For instance, the mechanism underlying this defect inspired phase-transition in ferroelectrics is not clear. Consequently, to understand the intrinsic behaviors and phase-transitions of defected ferroelectric materials in details, this work investigated the defect-driven ferroelectric phase-transition under the presence of external electric field. The modified Heisenberg model (in a form of discrete vector model) was considered and simulated via Monte Carlo simulation. Metropolis algorithm [8, 9] was performed to update

Received July 23, 2013; in final form January 12, 2014.

*Corresponding author. E-mail: yongyut_laosiritaworn@yahoo.com

[157]/1

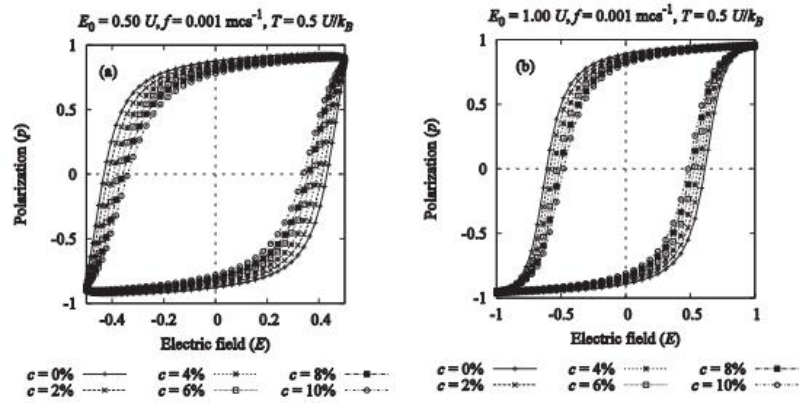


Figure 1. The hysteresis loops simulated at (a) $E_0 = 0.50 U$ and (b) $E_0 = 1.00 U$ with varying defect concentration $c = 0, 2, 4, 6, 8, 10\%$, but fixing frequency $f = 0.001 \text{ mcs}^{-1}$ and temperature $T = 0.5 U/k_B$.

the two dimensional ferroelectric film. DIFFOUR type interaction was used to study the dipole configuration and ferroelectric behaviors. Vacancy defects were introduced into the ferroelectric system to observe temperature and field parameters dependent of polarization characteristic and how defect concentration plays its role on the dynamic phase-transition.

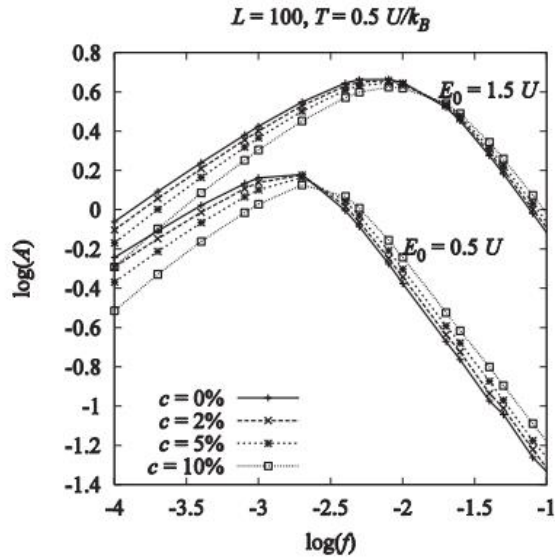


Figure 2. The frequency dependence of hysteresis loop area with various $c = 0, 2, 5, 10\%$.

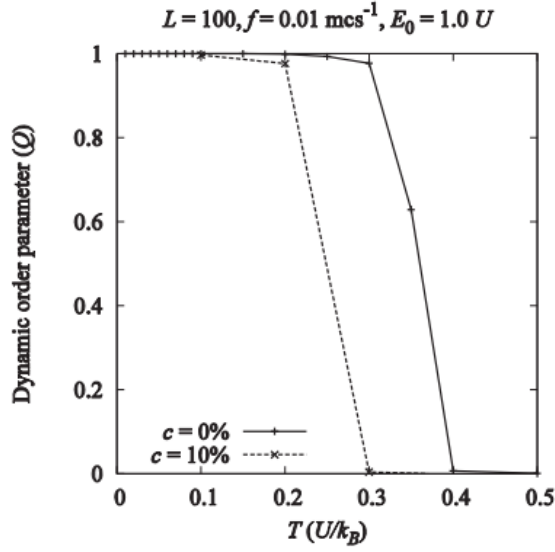


Figure 3. The temperature dependence of dynamic order parameter simulated at frequency $f = 0.01 \text{ mcs}^{-1}$ and $E_0 = 1.0 U$.

2. Methodologies

In the study of two-dimensional defected ferroelectric film, the modified Heisenberg model (discrete vector model) with DIFFOUR type interaction was considered. The Hamiltonian was written as [10, 11]

$$H = \sum_i \left(\frac{P_0^2}{2m} - \frac{a}{2} u_i^2 + \frac{b}{2} u_i^4 \right) - \sum_{\langle ij \rangle} U_{ij} \vec{u}_i \cdot \vec{u}_j - \vec{E}(t) \cdot \sum_i \vec{u}_i, \quad (1)$$

where $P_0^2/2m$ is the kinetic energy, \vec{u}_i denotes the ferroelectric dipole vector at site i , U_{ij} represents the ferroelectric interaction between dipole vectors \vec{u}_i and \vec{u}_j , a and b are the double-well potential parameters, $\langle ij \rangle$ means the summation taking over only the first neighbor pairs of dipoles and $\vec{E}(t) = E(t)\hat{z} = E_0 \sin(2\pi f)\hat{z}$ refers to an external electric field acting only on the z -component, where E_0 and f are field amplitude and frequency respectively. Eq. (1) can be simplified by setting $P_0^2/2m$ and $|\vec{u}_i|$ as constants, and $U_{ij} = U$ as a unit of energy. Therefore [12]

$$H = -U \sum_{\langle ij \rangle} \hat{u}_i \cdot \hat{u}_j - E(t) \sum_i u_{iz}, \quad (2)$$

where \hat{u}_i is a unit vector having one of the possible 14 ferroelectric dipole directions (8 from rhombohedral and 6 tetragonal structures), u_{iz} refers to the z -component dipole at site i . In this work, the magnitude of each dipole was set to one where its real magnitude was absorbed into U , and the unit of temperature T and electric field E were U/k_B and U respectively, where k_B is the Boltzmann's constant. The system was prepared by assigning random available

directions to all ferroelectric dipoles with a total number of $N' = (1 - c)N$ and $N = L \times L$ sites, where L is the linear system size, and c denotes the defect concentration (non-electric-sites) of system. $L = 100$ was chosen and $c = 0, 2, 4, 5, 6, 8, 10\%$ were included to the system with periodic boundary condition. In updating the dipole configuration, a random dipole was chosen and assigned a new direction (from 14 possible directions) with the Metropolis probability i.e. $p_M = \exp(-\Delta H_i(t)/k_B T)$, where $\Delta H_i(t)$ is the change in energy due to the update at site i and time t . The unit of time was defined as the Monte Carlo step per site (mcs); 1 mcs is equivalent to N' trial updates. Then in each simulation, the polarization per dipole was calculated i.e. $p(t) = (1/N') \sum_i u_{iz}(t)$ to create the hysteresis loops. The first 1000 loops were discarded for steady state condition, and next 2000 loops were used to average the hysteresis loop area $A = \oint p dE$, and the dynamic order parameter $Q = (1/P) \int_0^P p(t) dt$ where $P = 1/f$ is the field-period. Q was used to investigate the dynamic phase transition; $Q \neq 0$ for dynamic ferroelectric phase and $Q = 0$ for dynamic paraelectric phase.

3. Results and Discussions

In this work, since the number of dipole flipping is an integer and the number of data points recorded per hysteresis loop is 100 points; therefore the allowed frequency has to satisfy the condition $\frac{N'}{100f}$ being an integer. From the simulation results, the hysteresis characteristics which are hysteresis loop area and dynamic order parameter profiles, under defect structures, were obtained. From Fig. 1(a) and 1(b), the hysteresis loops were simulated at $E_0 = 0.5 U$ and $E_0 = 1.0 U$, $T = 0.5 U/k_B$ and $f = 0.001 \text{ mcs}^{-1}$. It is found that at higher defect concentration c , slimmer hysteresis loops are observed since the absence of some dipoles ceases ferroelectric interaction. The energy dissipation associated to dipole switching also decreases. Moreover, the frequency dependence of hysteresis loop area for various c was obtained as shown in Fig. 2. At low frequencies (i.e. frequencies smaller than the one that yields highest hysteresis area), the higher defect concentration gives smaller hysteresis loop area due to weaker ferroelectric interaction and smaller phase-lag (as higher period allows more time for dipole switching with electric field. However, for high frequencies, the higher defect concentration gives the larger hysteresis loop area due to high frequency induces high phase-lagging between polarization and field signals. Hence, the hysteresis loop becomes asymmetric (not shown) and the area ceases. Nevertheless, higher defect concentration ceases ferroelectric interaction and reduces the overall phase-lag, so the loop becomes more symmetric and the area increases. Moreover, effects of defect on dynamic order parameter were also investigated as illustrated in Fig. 3. It shows that the dynamic phase transition temperature (where slope is maximum) decreases with increasing defect concentration.

4. Conclusion

The properties of the two dimensional defected ferroelectric film were investigated through its hysteresis loop using the modified Heisenberg model with DIFFOUR interaction, Monte Carlo simulation, and the Metropolis algorithm. The hysteresis loop area and dynamic order parameters were extracted. This study shows how defect concentrations affect the hysteresis shape, hysteresis loop area and dynamic order parameters.

Acknowledgment

This work was supported by the Graduate School, Chiang Mai University, and Maejo University Phrae Campus.

References

1. J. F. Scott, *Ferroelectric Memories*. Berlin: Springer-Verlag (2002).
2. J. F. Scott and M. Dawber, Oxygen-vacancy ordering as a fatigue mechanism in perovskite ferroelectrics. *Appl. Phys. Lett.*, **76**, 3801–3803 (2000).
3. A. Murayama, K. Hyomi, J. Eickmann, and C. M. Falco, Brillouin study of long-wavelength spin waves in quasimonatomic Co films with uniaxial perpendicular magnetic anisotropy. *Phys. Rev. B*, **61**, 8984–8992 (2000).
4. J. B. G. Potter, V. Tikare, and B. A. Tuttle, Monte Carlo simulation of ferroelectric domain structure and applied field response in two dimensions. *J. Appl. Phys.*, **87**, 4415–4424 (2000).
5. J. M. Liu and Z. G. Liu, A Monte-Carlo approach of domain switching in ferroelectric Potts lattice under external electric field. *Materials Letters*, **36**, 17–23 (1998).
6. S. Nambu and D. A. Sagala, Domain formation and elastic long-range interaction in ferroelectric perovskites. *Phys. Rev. B*, **50**, 5838–5847 (1994).
7. W. Cao and L. E. Cross, Theory of tetragonal twin structures in ferroelectric perovskites with a first-order phase transition. *Phys. Rev. B*, **44**, 5–12 (1991).
8. K. Binder and D. W. Heermann, *Monte Carlo Simulation in Statistical Physics: An Introduction*. 5th ed., Berlin Heidelberg: Springer-Verlag (2010).
9. N. Metropolis, A. W. Rosenbluth, M. N. Rosenbluth, A. H. Teller, and E. Teller, Equation of state calculations by fast computing machines. *J. Chem. Phys.*, **21**, 1087–1092 (1953).
10. J. M. Liu, W. M. Wang, Z. G. Liu, H. L. Chan, and C. L. Choy, Dynamic hysteresis in ferroelectric systems: experiment and Monte Carlo simulation. *Appl. Phys. A*, **75**, 507–514–514 (2002).
11. T. Janssen and J. A. Tjon, One-dimensional model for a crystal with displacive modulation. *Phys. Rev. B*, **24**, 2245–2248 (1981).
12. Y. Laosiritaworn, Monte Carlo Investigation of Ferroelectric Properties in Thin Films. *Key Eng. Mater.*, **421–422**, 177–181 (2010).

Effects of Oxygen Vacancy on Ferroelectric Hysteresis under External Electric and Stress Fields

S. SRINOI,¹ R. YIMNIRUN,² AND Y. LAOSIRITAWORN^{1,*}

¹Department of Physics and Materials Science, Faculty of Science, Chiang Mai University, Chiang Mai 50200, Thailand

²School of Physics, Institute of Science, Suranaree University of Technology, Nakhon Ratchasima 30000, Thailand

Effects of oxygen vacancies on properties of ferroelectric materials were investigated through their hysteresis characteristics using Monte Carlo simulation. The purpose of this work is to study the roles of oxygen vacancy in ferroelectrics. The 2D four-state Potts model was considered for dipole switching. Under the application of external electric and stress fields, for both static and periodic field conditions, the electrical polarization and strain were numerically calculated with varying stress field and oxygen-vacancy probability (or concentration). It was found that, with or without an applied stress, the coercivity, remnant and saturation of the ferroelectric and elastic properties decrease with increasing oxygen vacancies. Moreover, under an applied periodic stress, the shapes of strain-electric-field butterfly loops were found similar to those obtained from applying the combination of two static stresses.

Keywords Oxygen vacancy; Monte Carlo simulation; Potts model; hysteresis loop

1. Introduction

A hysteresis loop can be characterized by a history-independent path. It naturally occurs in many physical systems under some circumstances such as the application and the removal of an electric field, a magnetic field, or a stress field. Hysteresis also exhibits the non-linearity properties of systems. Therefore, to clearly understand the behaviors of systems, some hysteresis loops that occur in many materials are extensively investigated. To better understand some physical properties, such as dielectricity, piezoelectricity, or pyroelectricity, ferroelectric materials—one of vital components widely used in electronic devices, nonvolatile memory media, and tunable dielectrics—are widely investigated through their hysteresis loops under various conditions [1-7]. Below the transition temperature, ferroelectrics, in general, can change from high-symmetry structure to low-symmetry structure with the occurrence of spontaneous polarization and spontaneous strain-lattice distortion induced by the spontaneous polarization. Additionally, the change in the direction of spontaneous polarization under high electromechanical loadings causes the hysteresis loops in ferroelectrics. Polarization switching should be considered to take full advantage of ferroelectric materials. Therefore, in this work, the structural effects such as oxygen vacancies on the properties of ferroelectrics were investigated through their hysteresis loops.

Received in final form June 1, 2013.

*Corresponding author; E-mail: yongyut_laosiritaworn@yahoo.com

The responses of ferroelectric materials under the electric and stress fields were intensively investigated in previous works with many different conditions, for example, the combination of periodic electric field and static stress field [8], periodic stress field and static electric field [9], or periodic electric and stress fields [10], etc. Oxygen vacancy—one kind of common structural defects in ferroelectrics—can result from many different oxidation processes. This vacancy influences the ferroelectric properties [11, 12]. It is thus important to understand the roles and mechanisms of the oxygen vacancies on ferroelectric properties.

2. Methodology

It is suitable to use the 2D four-state Potts model in simulating the ferroelectric properties due to the coexistence of both 90° and 180° domain wall [13]. Its dipoles have four different alignments and are mutually perpendicular to each other. Therefore, in this work, a two-dimensional array of $N = N_x N_z$ cells on the xz plane was purposed, where N_x and N_z are the number of cells along the x - and z -directions, respectively. Each cell can be also represented by a tetragonal rectangle [9]. A dipole at a cell index i ($0 < i \leq N$), was replaced by a spin matrix \hat{S}_i , which takes one of the four possible directions as the followings

$$\hat{S}_i = \hat{S}_A = \begin{bmatrix} 1 \\ 0 \end{bmatrix} \text{ along } +z \text{ direction (upward),} \quad (1a)$$

$$\hat{S}_i = \hat{S}_B = \begin{bmatrix} 0 \\ 1 \end{bmatrix} \text{ along } +x \text{ direction (left),} \quad (1b)$$

$$\hat{S}_i = \hat{S}_C = \begin{bmatrix} -1 \\ 0 \end{bmatrix} \text{ along } -z \text{ direction (downward),} \quad (1c)$$

or

$$\hat{S}_i = \hat{S}_D = \begin{bmatrix} 0 \\ -1 \end{bmatrix} \text{ along } -x \text{ direction (right),} \quad (1d)$$

where A , B , C or D represents the four possible states. As the direction of the dipole is relevant to the orientation of the tetragonal rectangle, the ferroelastic strain state $\hat{\varepsilon}_i^F$ of a cell can be defined as the following equations [7, 9]

$$\hat{\varepsilon}_i^F = \begin{bmatrix} \varepsilon_0 \\ -\varepsilon_0/2 \end{bmatrix} \text{ (state } A \text{ or } C), \quad (2a)$$

$$\hat{\varepsilon}_i^F = \begin{bmatrix} -\varepsilon_0 \\ \varepsilon_0/2 \end{bmatrix} \text{ (state } B \text{ or } D), \quad (2b)$$

where ε_0 is the constant strain of tetragonal cell along the elongated edge.

From a typical 3D tetragonal structure of a perovskite-type ferroelectric material, the O^{2-} ions located at the center of six faces can be represented into a 2D rectangle model with four faces: top, left, bottom, and right. Therefore, the oxygen vacancies were laid at one of possible four sides of a tetragonal cell. At a cell i , the presence of an oxygen vacancy can be represented as the following expressions [14, 15]

$$\hat{V}_i = \begin{bmatrix} 0 \\ 0 \end{bmatrix} \text{ (non-vacancy),} \quad (3a)$$

$$\hat{V}_i = \begin{bmatrix} 1 \\ 0 \end{bmatrix} \quad (\text{vacancy at top side}), \quad (3b)$$

$$\hat{V}_i = \begin{bmatrix} 0 \\ 1 \end{bmatrix} \quad (\text{vacancy at left side}), \quad (3c)$$

$$\hat{V}_i = \begin{bmatrix} -1 \\ 0 \end{bmatrix} \quad (\text{vacancy at bottom side}), \quad (3d)$$

$$\hat{V}_i = \begin{bmatrix} 0 \\ -1 \end{bmatrix} \quad (\text{vacancy at right side}), \quad (3e)$$

By considering the mechanical energy density without the anisotropic switching, a ferroelectric material is composed of many energy terms i.e.

$$H = H_0 + \sum_i H_{V1} \hat{V}_i^T \hat{S}_i - \sum_{\langle ij \rangle} H_{V2} \{ \hat{V}_i^T \hat{V}_j \} \{ \hat{S}_i^T \hat{S}_j \}, \quad (4)$$

where H_0 is the Hamiltonian of a spin system without any oxygen vacancies, the symbol $\sum_{\langle ij \rangle}$ is the summation over the nearest neighbors, H_{V1} refers to the coupling interaction between oxygen vacancies and dipoles, H_{V2} is the coupling strength between the distorted cells and the neighboring dipoles. \hat{X}^T is the transpose matrix of \hat{X} which has the following form $\hat{X} = \begin{bmatrix} X_z \\ X_x \end{bmatrix}$, where X_z and X_x are the components along to z - (longitudinal) and x - (transverse) directions, respectively ($\hat{X} = \hat{V}$ or \hat{S}). Its unit is absorbed into H_{V1} or H_{V2} , and each term in Eq. (4) was also redefined as the energy unit. For the absence of oxygen vacancies, the system Hamiltonian can be written as

$$H_0 = - \sum_{\langle ij \rangle} J \hat{S}_i^T \hat{S}_j - P_S \sum_i \hat{E}_i^T \hat{S}_i - \alpha \sum_{\langle ij \rangle} \hat{\epsilon}_i^{F^T} \hat{\epsilon}_j^F - \sum_i \hat{\sigma}^T \hat{\epsilon}_i, \quad (5)$$

where J and α are the dipole-coupling coefficient and ferroelastic-strain-coupling coefficient, respectively, P_S is the magnitude of the dipole moment of a cell, \hat{E} and $\hat{\sigma}$ are the periodic external electric and stress fields. Similarly, J and α are redefined as the energy unit by absorbing the unit of \hat{S} and $\hat{\epsilon}$, respectively. Therefore, the unit of the electric field was defined as J and temperature as J/k_B , where k_B is the Boltzmann's constant. If both external electric and stress fields are uniform in space, and have only longitudinal forms (z -direction) and initially in phase, they can be expressed as

$$\hat{E} = \begin{bmatrix} E_z \\ E_x \end{bmatrix} = \begin{bmatrix} E_0 \sin(2\pi f_E t) \\ 0 \end{bmatrix}, \quad (6)$$

and

$$\hat{\sigma} = \begin{bmatrix} \sigma_z \\ \sigma_x \end{bmatrix} = \begin{bmatrix} \sigma_0 \sin(2\pi f_\sigma t) \\ 0 \end{bmatrix}, \quad (7)$$

where E_0 and σ_0 are the electric and stress field amplitudes, for a tensile stress, $\sigma_z = \sigma_0$ ($\sigma_0 > 0$ for a tensile stress and $\sigma_0 < 0$ for a compressive stress), t is the time which is scaled in term of number of Monte Carlo steps (mcs), f_E and f_σ are the electric and stress field frequencies, respectively, which have the unit of mcs^{-1} . In the simulation, the numbers of data (or points) per a loop used to generate a hysteresis loop rely on one field frequency (or one period). Under a static and periodic field, a hysteresis loop can be created

easily by these points. However, two different field frequencies may lead to their different numbers of points per a loop. It is not quite suitable to plot a hysteresis loop and compare using different numbers of points. Therefore, in this work, $f_E = f_\sigma = f$ was considered as suggested in previous works [8, 16]. In Eq. (5), $\hat{\varepsilon}_i$ is the total strain which can be divided into two parts (without field-induced strain) as,

$$\hat{\varepsilon}_i = \hat{\varepsilon}_i^F + \hat{\varepsilon}_i^{el}, \quad (8)$$

where $\hat{\varepsilon}_i^{el}$ is the elastic strain determined by the elastic property of the material. For a small stress, it was found that

$$\hat{\varepsilon}_i^{el} = \frac{1}{Y} \begin{bmatrix} 1 & -\nu \\ -\nu & 1 \end{bmatrix} \begin{bmatrix} \sigma_z \\ \sigma_x \end{bmatrix}. \quad (9)$$

Here, Y and ν are the Young's modulus and Poisson ratio, respectively.

In preparing the system, each spin was placed at any sites randomly with possible directions as described previously. Consequently, the system was initially unpoled. The ferroelastic strain states were also automatically initialized since both spin states and ferroelastic strain states were associated as Eqs. (1a–1d) and Eqs. (2a–2b). In simulating the existence of oxygen vacancies, the total number of vacancies $N_V = cN$, where c is the oxygen-vacancy probability or vacancy concentration, was defined where, for each cell, the vacancies randomly distributed on possible positions as mentioned in Eqs.(3a–3e). The presence of oxygen vacancy at different sides of a cell is governed by the probability p_T (top), p_B (bottom), p_L (left) and p_R (right). These probabilities follow the condition $p_T + p_L + p_B + p_R = 1$. Moreover, periodic and free boundary conditions were employed along x - and z -directions, respectively.

After providing the initial configuration of system, a spin was randomly selected for a trial rotation which is determined by the Metropolis algorithm [17]. The macroscopic polarization and strain were calculated using the following expressions

$$P_z = \frac{P_S \sum_i \hat{n}^T \hat{S}_i}{N}, \quad (10)$$

$$\varepsilon_z = \frac{\sum_i \hat{n}_i^T (\hat{\varepsilon}_i - \hat{\varepsilon}_i^0)}{N}, \quad (11)$$

and

$$\varepsilon_x = \frac{\sum_i \hat{q}^T (\hat{\varepsilon}_i - \hat{\varepsilon}_i^0)}{N}, \quad (12)$$

where $\hat{n} = \begin{bmatrix} 1 \\ 0 \end{bmatrix}$ and $\hat{q} = \begin{bmatrix} 0 \\ 1 \end{bmatrix}$ denote the longitudinal and transverse unit matrix, respectively, and $\hat{\varepsilon}_i^0$ is the initial strain matrix for each cell. Then the ferroelectric hysteresis loops were obtained to investigate their properties through the hysteresis area as the following expression:

$$A = \oint P_z dE, \quad (13)$$

3. Results and Discussions

The objective of this work is to study the roles of oxygen vacancies on the ferroelectric properties under the combination of the external electric and stress fields. The orientation of dipoles and the distribution of oxygen vacancies were assumed to be uniform and isotropic. Moreover, the coupling coefficient J was treated to be isotropic [15]. Therefore, the following numerical parameters were purposed: $N_x = 200$, $N_z = 80$, $E_0 = 1.2$, $\sigma_0 = 0.5$, $P_S = 1.0$, $\varepsilon_0 = 0.5$, $f = 0.0025$, $H_{V1} = 5.0$, $H_{V2} = 2.0$, $Y = 2.0$, $\nu = 0.3$, $J = 1$, $\alpha = 0.8$, $p_T = p_L = p_B = p_R = 0.25$, and temperature $T = 1.0$. This work studied the ferroelectric behaviors under external factors as followings: (1) periodic external electric field and free stress field, (2) periodic external electric field and static stress field, and (3) periodic external electric and stress fields. To investigate how ferroelectric hysteresis responds to the vacancy concentration c under these mentioned conditions, the P_z - E_z hysteresis and ε_z - E_z butterfly loops were evaluated numerically. Under varying vacancy concentration c , the P_z - E_z hysteresis loops with free ($\sigma_z = 0$), longitudinal tensile ($\sigma_z = 0.5$), longitudinal compressive ($\sigma_z = -0.5$) and periodic stresses ($\sigma_z = \sigma_0 \sin(2\pi ft)$) were shown in Figs. 1(a), 1(b), 1(c) and 1(d), respectively. They all show that the responses of hysteresis

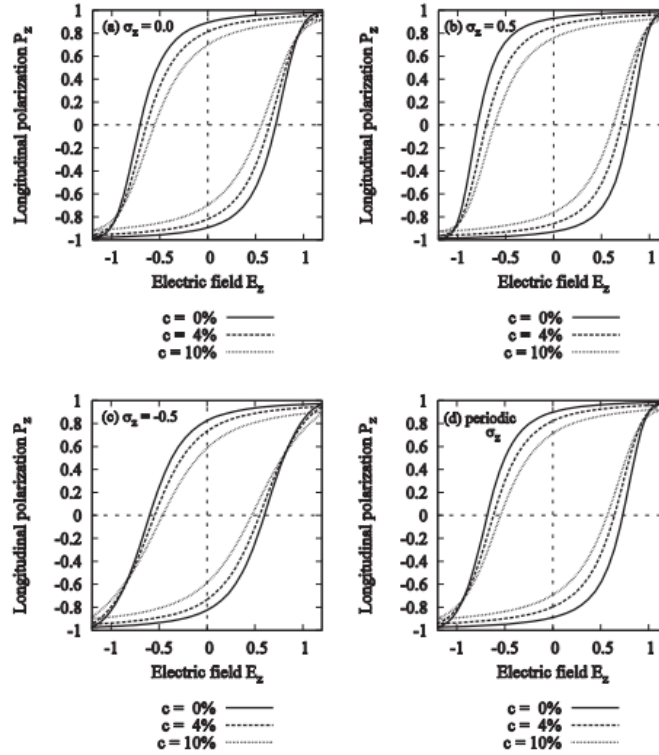


Figure 1. P_z - E_z hysteresis loops with $c = 0, 4$, and 10% simulated at (a) $\sigma_z = 0$, (b) $\sigma_z = 0.5$, (c) $\sigma_z = -0.5$ and (d) $\sigma_z = \sigma_0 \sin(2\pi ft)$.

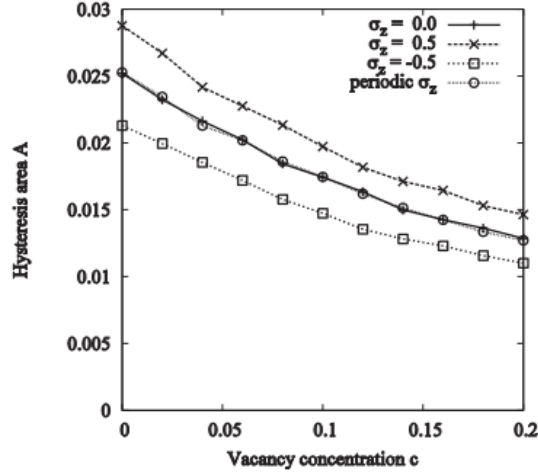


Figure 2. Hysteresis area versus vacancy concentration simulated at $\sigma_z = 0.0, 0.5, -0.5$, and $\sigma_0 \sin(2\pi ft)$.

loops are quite similar, that is, both the coercive field and remnant longitudinal polarization reduces with increasing vacancy concentration. Since the enhancement or reduction of longitudinal polarization depends on the number of dipoles being in A or C states (z -direction), dipole switching into A or C states is inhibited from increasing of oxygen vacancies either with or without applied stresses. On the other hand, the number of B or D states (x -direction) increases with increasing oxygen vacancies.

Under a longitudinal tensile stress and periodic z -axis electric field, each dipole tends to align in z -direction. Therefore, A or C states are enhanced by the existence of a longitudinal tensile stress, compared to free or a longitudinal compressive stress. Moreover, the number of dipoles oriented in z -direction can be also represented by the P_z - E_z hysteresis area which refers to the energy dissipated in switching dipoles. Therefore, the hysteresis area increases with increasing number of dipoles in z -direction. The previous work showed that the remnant polarization decreases with a compressive stress [18]. Additionally, the mentioned explanation is confirmed by evidences in Fig. 2. However, the obtained results under a periodic external stress are similar to those under free stress because average external stress over a cycle vanishes.

Like the longitudinal polarization versus electric-field curves, both longitudinal and transverse strains driven by a periodic electric field were evaluated. Then the strain-electric-field butterfly loops were obtained as shown in Fig. 3, which has the same conditions as Fig. 1. The results show the saturated longitudinal strains decrease with increasing oxygen vacancies. The same goes for transverse strain (not shown). It was also found that the change in longitudinal strain (difference between the lowest and saturated values) over a cycle is smallest for a longitudinal tensile stress $\sigma_z = 0.5$ (Fig. 3(b)), because most dipoles are forced to align along the z -direction under this stress. As most dipoles prefer to lay in x -direction under a longitudinal compressive stress $\sigma_z = -0.5$, the change in longitudinal strain is the largest (Fig. 3(c)). However, under the considered periodic external stress (Fig. 3(d)), it was found that $\sigma_{z,\min} = \sigma_0 = -0.5$ and $\sigma_{z,\max} = \sigma_0 = 0.5$. The shapes of strain-electric-field butterfly loops were found similar to those obtained from applying the

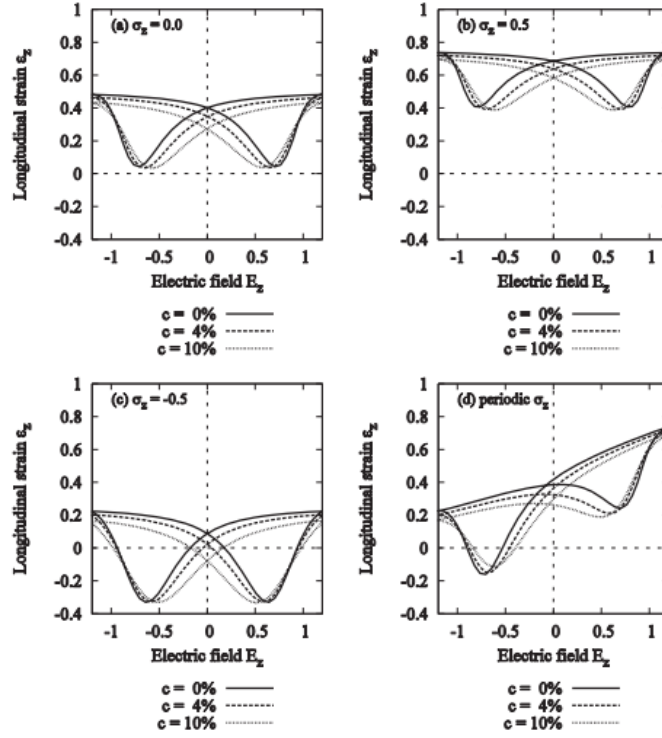


Figure 3. ϵ_z - E_z hysteresis loops with $c = 0, 4,$ and 10% simulated at (a) $\sigma_z = 0$, (b) $\sigma_z = 0.5$, (c) $\sigma_z = -0.5$ and (d) $\sigma_z = \sigma_0 \sin(2\pi ft)$.

combination of two static stresses. Specifically, there are two saturation strains: the one in the range $E_z = [0, E_0]$ is equivalent to a static stress $\sigma_z = 0.5$ and the other in the range $E_z = [-E_0, 0]$ is consistent with a static stress $\sigma_z = -0.5$.

4. Conclusions

The effects of oxygen vacancies on the ferroelectric materials under the combination of external electric and stress fields were investigated through their hysteresis loops using a Monte Carlo method. The 2D four-state Potts model was considered for switching dipoles. Under a longitudinal tensile stress, the hysteresis area becomes larger while the change in longitudinal strain becomes smaller than that under a free, longitudinal tensile, longitudinal compressive, and periodic stresses.

Funding

The authors would like to acknowledge financial supports from the Graduate School of Chiang Mai University and Development and Promotion of Science and Technology Talents Project (DPST).

References

1. S. Srinoi and Y. Laosiritaworn, The role of vacancy defects on the dynamic hysteresis properties of ferroelectric thin films: Monte Carlo simulation with the DIFFOUR model. *Ferroelectrics*. **414**, 140–146 (2011).
2. Y. Laosiritaworn, K. Kanchiang, A. Ngamjarrojana, R. Yimnirun, R. Guo, and A. S. Bhalla, The Debye dielectric behavior of mixed normal and relaxor-ferroelectrics: Monte Carlo investigation. *Ferroelectrics*. **401**, 239–245 (2010).
3. Y. Laosiritaworn, K. Kanchiang, R. Yimnirun, R. Guo, and A. S. Bhalla, Monte Carlo investigation of mixed normal and relaxor ferroelectrics. *Ferroelectrics*. **382**, 28–35 (2009).
4. Y. Laosiritaworn, K. Kanchiang, R. Yimnirun, R. Guo, and A. S. Bhalla, Monte Carlo simulations of relaxor ferroelectric dielectric permittivity in films structure. *Ferroelectrics*. **380**, 169–176 (2009).
5. Y. Laosiritaworn, S. Ananta, J. Poulter, and R. Yimnirun, Monte Carlo investigation of hysteresis properties in ferroelectric thin-films under the effect of uniaxial stresses. *Ceram. Int.* **35**, 181–184 (2009).
6. C. H. Ahn, K. M. Rabe, and J. M. Triscone, Ferroelectricity at the nanoscale: local polarization in oxide thin films and heterostructures. *Science*. **303**, 488–491 (2004).
7. W. F. Li and G. J. Weng, A theory of ferroelectric hysteresis with a superimposed stress. *J. Appl. Phys.* **91**, 3806–3815 (2002).
8. D. Zhou and M. Kamlah, High-field dielectric and piezoelectric performance of soft lead zirconate titanate piezoceramics under combined electromechanical loading. *J. Appl. Phys.* **96**, 6634–6641 (2004).
9. H. X. Cao, V. C. Lo, and W. W. Y. Chung, Investigation of electromechanical properties in ferroelectric thin films using Monte Carlo simulation. *J. Appl. Phys.* **99**, 024103 (2006).
10. M. Mitrovic, G. P. Carman, and F. K. Straub, Response of piezoelectric stack actuators under combined electro-mechanical loading. *Int. J. Solids. Struct.* **38**, 4357–4374 (2001).
11. Y. Wang, K. F. Wang, C. Zhu, T. Wei, J. S. Zhu, and J. M. Liu, Fatigue suppression of ferroelectric $\text{Pb}_{1-x}\text{Ba}_x(\text{Zr}_{0.52}\text{Ti}_{0.48})\text{O}_3$ thin films prepared by sol-gel method. *J. Appl. Phys.* **101**, 046104 (2007).
12. L. X. Zhang and X. Ren, In situ observation of reversible domain switching in aged Mn-doped BaTiO_3 single crystals. *Phys. Rev. B*. **71**, 174108 (2005).
13. V. Nagarajan, I. G. Jenkins, S. P. Alpay, H. Li, S. Aggarwal, L. Salamanca-Riba, A. L. Roytburd, and R. Ramesh, Thickness dependence of structural and electrical properties in epitaxial lead zirconate titanate films. *J. Appl. Phys.* **86**, 595–602 (1999).
14. K. T. Li and V. C. Lo, Simulation of oxygen vacancy induced phenomena in ferroelectric thin films. *J. Appl. Phys.* **97**, 034107 (2005).
15. V. C. Lo, Modeling the role of oxygen vacancy on ferroelectric properties in thin films. *J. Appl. Phys.* **92**, 6778–6786 (2002).
16. V. C. Lo, W. W. Y. Chung, and S. C. K. Chow, Simulation of electromechanical responses of ferroelectric ceramics driven by combined alternating electrical and mechanical loadings. *J. Appl. Phys.* **101**, 114111 (2007).
17. N. Metropolis, A. W. Rosenbluth, M. N. Rosenbluth, A. H. Teller, and E. Teller, Equation of state calculations by fast computing machines. *J. Chem. Phys.* **21**, 1087–1092 (1953).
18. D. Zhou, M. Kamlah, and D. Munz, Effects of uniaxial prestress on the ferroelectric hysteretic response of soft PZT. *J. Eur. Ceram. Soc.* **25**, 425–432 (2005).

CURRICULUM VITAE

Author's Name	Mr. Sittidet Srinoi
Date of Birth	4 March 1977
Place of Birth	Lopburi, Thailand
Education	2000 B.S. (Physics), Chiang Mai University 2003 M.S. (Physics), Chiang Mai University
Scholarship	1996-2003 Development and Promotion of Science and Technology Talents Project (DPST) 2007-2010 Development and Promotion of Science and Technology Talents Project (DPST)
Publications	Sittidet Srinoi and Yongyut Laosiritaworn, "The Role of Vacancy Defects on the Dynamic Hysteresis Properties of Ferroelectric Thin Films: Monte Carlo Simulation with the DIFFOUR model", Ferroelectrics, 414 , 2011, 140. S. Srinoi, K. Kanchiang, W. Laosiritaworn, R. Yimnirun, and Y. Laosiritaworn, "Ferroic Hysteresis Modeling" Int. Ferroelectrics, 131 , 2011, 202. Sittidet Srinoi and Yongyut Laosiritaworn, "Investigation of Temperature-Driven Ferroelectric Phase-Transition via Modified Heisenberg Model: The Monte Carlo Simulation", Adv. Mater. Res., 813 , 2013, 315. S. Srinoi and Y. Laosiritaworn, "Monte Carlo Investigation of Defect-Driven Ferroelectric Phase-Transition in Two Dimensional Defected Film", Int. Ferroelectrics, 156 , 2014, 1.

S. Srinoi, R. Yimnirun and Y. Laosiritaworn, “Effects of Oxygen Vacancy on Ferroelectric Hysteresis under External Electric and Stress Fields”, *Ferroelectrics*, **470**, 2014, 35.

Conferences

National:

S. Srinoi and Y. Laosiritaworn, “Phase Transition Investigation of Ferroelectric Materials via Modified XY Model in 2 Dimensions: Monte Carlo Simulation”, Siam Physics Congress, Kanchanaburi, Thailand (2010).

S. Srinoi and Y. Laosiritaworn, “Investigation of Temperature-Driven Ferroelectric Phase-Transition: The Monte Carlo Simulation”, Siam Physics Congress, Chonburi, Thailand (2011).

International:

S. Srinoi and Y. Laosiritaworn, “The Role of Vacancy Defects on the Dynamic Hysteresis Properties of Ferroelectric Thin Films: Monte Carlo Simulation with the DIFFOUR model”, The 10th Russia/CIS/Baltic/Japan Symposium on Ferroelectricity (RCBJSF-10), Yokohama, Japan (2010).

S. Srinoi and Y. Laosiritaworn, “Investigation of Temperature-driven Ferroelectric Phase-Transition via Modified Heisenberg Model: The Monte Carlo Simulation”, The 10th Russia/CIS/Baltic/Japan Symposium on Ferroelectricity (RCBJSF-10), Yokohama, Japan (2010).

